

Visualizing the Contribution of Keratin-14⁺ Limbal Epithelial Precursors in Corneal Wound Healing

Mijeong Park,¹ Alexander Richardson,¹ Elvis Pandzic,² Erwin P. Lobo,³ Renee Whan,² Stephanie L. Watson,⁴ J. Guy Lyons,^{5,6,7} Denis Wakefield,¹ and Nick Di Girolamo^{1,*}

¹Mechanisms of Disease and Translational Research, School of Medical Sciences, Faculty of Medicine, University of New South Wales, Sydney, NSW 2052, Australia

²Biomedical Imaging Facility, Mark Wainwright Analytical Centre, University of New South Wales, Sydney, NSW 2052, Australia

³School of Mathematics and Statistics, Faculty of Science, University of Sydney, Sydney, NSW 2006, Australia

⁴Save Sight Institute, University of Sydney, Sydney, NSW 2006, Australia

⁵Discipline of Dermatology, Bosch Institute, Charles Perkins Centre, University of Sydney, Sydney, NSW 2006, Australia

⁶Immune Imaging, Centenary Institute, Sydney, NSW 2006, Australia

⁷Cancer Services, Royal Prince Alfred Hospital, Sydney, NSW 2006, Australia

*Correspondence: n.digirolamo@unsw.edu.au

<https://doi.org/10.1016/j.stemcr.2018.11.014>

SUMMARY

It is thought that corneal epithelial injuries resolve by leading-edge cells “sliding” or “rolling” into the wound bed. Here, we challenge this notion and show by real-time imaging that corneal wounds initially heal by “basal cell migration.” The K14CreER^{T2}-Confetti multi-colored reporter mouse was employed to spatially and temporally fate-map cellular behavior during corneal wound healing. Keratin-14⁺ basal epithelia are forced into the wound bed by increased population pressure gradient from the limbus to the wound edge. As the defect resolves, centripetally migrating epithelia decelerate and replication in the periphery is reduced. With time, keratin-14⁺-derived clones diminish in number concomitant with their expansion, indicative that clonal evolution aligns with neutral drifting. These findings have important implications for the involvement of stem cells in acute tissue regeneration, in key sensory tissues such as the cornea.

INTRODUCTION

The cornea is the most anterior tissue of the eye, and its transparency is critical for vision. The outermost layer consists of a stratified squamous epithelium that protects against fluid loss, microbial invasion, ultraviolet radiation, and physical and chemical trauma (Di Girolamo, 2015; Richardson et al., 2016). Stem cells of the cornea reside in an annular transition zone known as the limbus and are otherwise known as limbal epithelial stem cells (LESCs). LESCs give rise to transit amplifying cells (TACs) that have high but limited proliferative potential, and subsequently terminally differentiated cells, which are exfoliated from the ocular surface. LESCs have important functional traits including an ability to self-renew, cycle slowly, and divide symmetrically and asymmetrically to produce daughter SCs or TACs (Beebe and Masters, 1996; Castro-Muñozledo and Gómez-Flores, 2011; Lamprecht, 1990; Lobo et al., 2016). During homeostasis, the corneal epithelium is continuously replenished in accord with the XYZ hypothesis, in which desquamating superficial cells (Z) must be replenished by proliferating basal cells (X) that migrate in a centripetal direction (Y) (Thoft and Friend, 1983). Under these conditions, the centripetal velocity of murine corneal epithelia ranges from 10 to 26 $\mu\text{m}/\text{day}$ (Buck, 1985; Di Girolamo et al., 2015; Nagasaki and Zhao, 2003). Upon injury, cell displacement is accelerated to fast-track healing,

and is likely influenced by proliferating LESCs and their early progeny (Lobo et al., 2016; Mort et al., 2009).

Following a superficial epithelial wound, three basic events transpire. In the initial phase, no active cell proliferation or migration occurs; instead, proteins are synthesized (Gipson and Kiorpes, 1982; Zieske and Gipson, 1986) and a temporary extracellular matrix is deposited (Fujikawa et al., 1981). Second, suprabasal wing cells “slide” into the wound bed to cover the defect (Crosson et al., 1986; Gipson and Kiorpes, 1982; Kuwabara et al., 1976). Finally, epithelial layers are restored by cells proliferating, differentiating, and stratifying (Lehrer et al., 1998; Stepp et al., 2014; Zhao et al., 2003).

After corneal epithelial debridement, cell migration is accelerated 40-fold compared with steady state (Kuwabara et al., 1976; Mort et al., 2009; Ramaesh et al., 2006), and slow-cycling LESCs can be stimulated to proliferate (Chung et al., 1999; Cotsarelis et al., 1989), thereby supporting the proposition that these cells provide the impetus to restore epithelial integrity. Although these studies offer fundamental mechanistic insights into cellular behavior, they are fraught with obvious limitations. A major challenge has been determining whether LESCs truly partake in corneal wound healing, and if so, what experimental paradigms could be employed to visualize their contribution in real-time. Despite attempts to resolve this shortcoming through the use of adenoviral vectors carrying a GFP

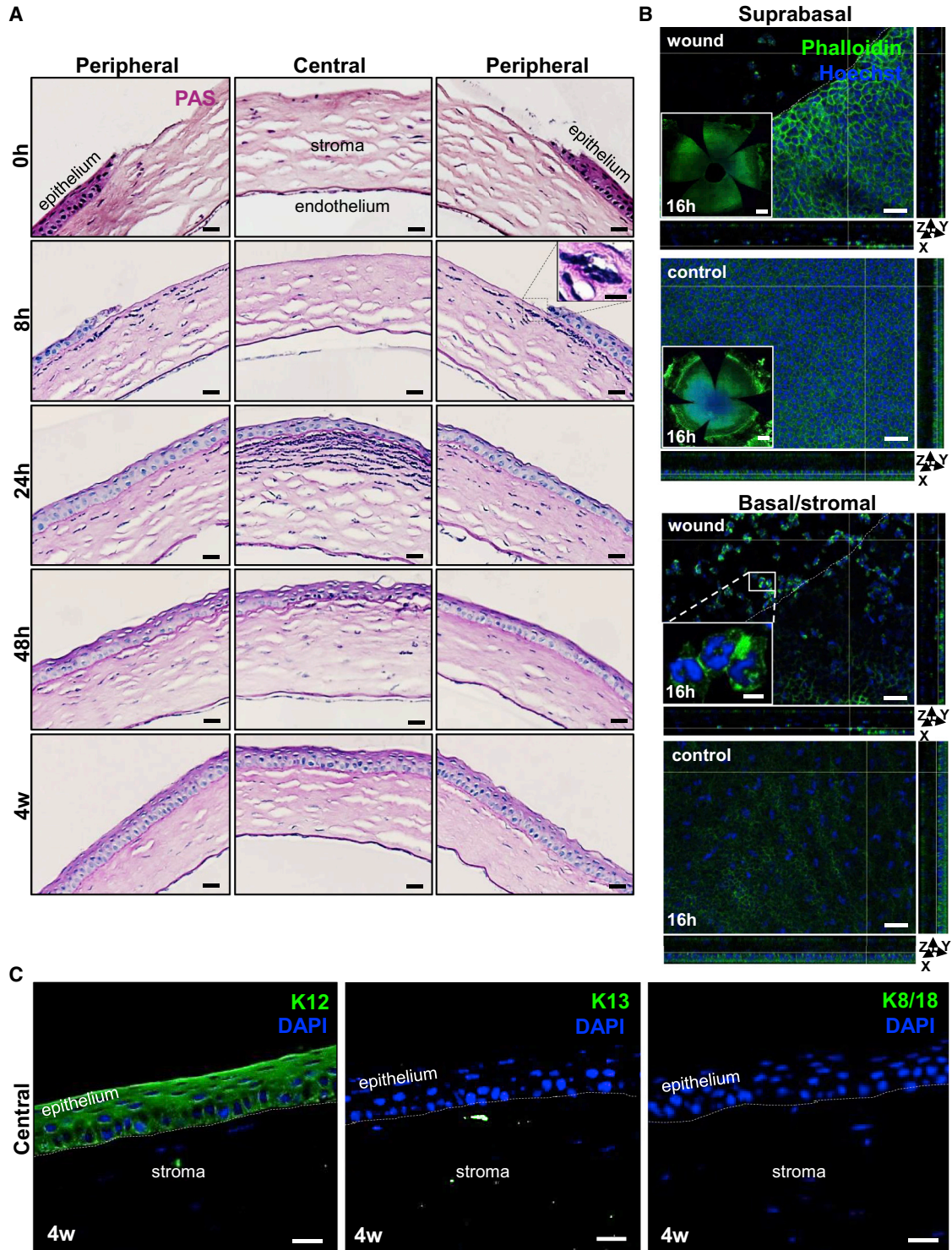


Figure 1. Restoration of a Phenotypically Normal Corneal Epithelium after Mechanical Debridement

(A) Seven-week-old WT mice ($n = 3$ /time point) had their right corneal epithelium mechanically debrided. Histological features of the central and peripheral cornea are displayed after staining 4- μ m sections with PAS at 0 hr, 8 hr, 24 hr, 48 hr and 4 weeks post injury. Scale bars represent 20 μ m. Inset presents a magnified view of the region encompassed by the hatched box and confirms a stromal neutrophilic infiltrate (scale bar, 10 μ m).

(legend continued on next page)



reporter (Danjo and Gipson, 2002) and non-specific transgenic reporters (Mort et al., 2009; Ramaesh et al., 2006), the origins of marked cells has been difficult to reconcile.

Herein, we employed the K14CreER^{T2}-Confetti (Confetti) mouse, which delivers stable, long-term labeling of keratin-14⁺ (K14⁺) limbal epithelia, along with their ensuing progeny. We provide the real-time spatial-temporal recordings of LESC during the initial phase of wound repair, and visualized elevated clonal activity emanating from the limbus, along with streaming basal limbal epithelia into the wound bed. After using bromodeoxyuridine (BrdU) labeling and applying a computational model, we confirmed that LESC proliferation generates population pressure in the periphery that drives basal cell displacement to seal the wound in a timely fashion. Finally, through the application of spatiotemporal image correlation spectroscopy (STICS) (Toplak et al., 2012), and after correcting for corneal curvature, we determined the velocity and direction of migrating clones during wound closure with greater precision.

RESULTS

Resolution of a Phenotypically Normal Corneal Epithelium after Mechanical Debridement

To assess the extent of epithelial debridement, we euthanized mice at regular intervals and examined their corneas after staining sections with periodic acid-Schiff (PAS) (Figure 1A). Corneas inflicted with a 2-mm wound displayed no central epithelium; however, the peripheral and limbal epithelium remained intact (Figure 1A, first row). At 8 hr post wounding, immune cells with multi-lobed nuclei infiltrated the stroma from the periphery (Figure 1A, second row, inset). Confocal microscopy on phalloidin-stained flat-mounted corneas at 16 hr post wounding suggested that these cells were mostly neutrophils (Li et al., 2006; Petrescu et al., 2007) confined to the superficial stroma (Figure 1B, second row, inset). By 24 hr post injury, the central cornea was covered by at least one layer of epithelia, stromal inflammation adjacent the regenerating epithelium was heightened, and the basement membrane was more pronounced (Figure 1A, third row, middle panel). Notably, this coincided with the disappearance of neutrophils from the periphery (Figure 1A, third row, left and right panels).

At 48 hr post wounding, the peripheral epithelium returned to near steady state, with reduced inflammation (Figure 1A, fourth row). Epithelial stratification was restored prior to 4 weeks post injury (Figure 1A, fifth row), with no signs of “conjunctivalization” (Huang and Tseng, 1991; Lin et al., 2013; Pajooohesh-Ganji et al., 2012). At this point in time, the regenerated central epithelium displayed corneal-specific K12 immunoreactivity but lacked conjunctival K13 and K8/18 expression (Figure 1C), indicating that the limbal barrier had not been breached and corneal epithelial regeneration likely ensued via proliferating LESC and/or TACs.

After staining specimens with phalloidin, we assessed cell morphology in and around the injury site just prior to wound closure (Figure 1B). At 16 hr post injury, cell size adjacent to the wound margin was significantly increased (Figure 1B [x-y plane] and Table S1); this was congruent with decreased cell density and epithelial thickness (Figure 1B, orthogonal views; x-z plane and y-z planes; and Table S1), implying the defect was covered by a monolayer or dual layer of epithelial cells that changed shape.

Accelerated Re-epithelialization of Corneal Wounds by K14⁺ Limbal Progenitor-Derived Clones

One advantage of utilizing an inducible transgenic model is the ability to visualize clonal evolution and expansion during wound healing in real time with intra-vital microscopy. However, to confirm that the genetic alterations in Confetti mice did not alter the wound-healing response, we compared wound-closure rates with those of wild-type (WT) mice. Fluorescein staining demonstrated that epithelial defects in Confetti (Figure 2A) and WT (not shown) mice healed at near identical rates (Figure 2C; $p = 0.964$) and were generally closed by 24–48 hr. The percentage wound closure at 8, 16, and 24 hr in Confetti mice was $79.0\% \pm 6.9\%$, $33.9\% \pm 9.9\%$, and $25.2\% \pm 4.8\%$, respectively, which was comparable with $84.6\% \pm 15.9\%$, $42.3\% \pm 9.8\%$, and $36.6\% \pm 18.1\%$ in WT mice (Figure 2C).

Following epithelial debridement, fluorescent patches derived from K14⁺ transgenic cells emerged from the limbus in wounded eyes (Figure 2B), and within 1 week developed into multi-colored clonal streaks that migrated at $19.8 \pm 3.7 \mu\text{m/hr}$ (Figure 2D) and persisted beyond 8 weeks post injury (Figure 2B). Fluorescent clones were displaced $180.5 \pm 42.0 \mu\text{m}$, $374.1 \pm 135.4 \mu\text{m}$, $574.1 \pm 86.3 \mu\text{m}$,

(B) Phalloidin (green)-stained flat-mounted whole corneas at 16 hr post wounding and control ($n = 5/\text{group}$). White hatched lines demarcate the wound margin. y-z and x-z planes display epithelial thickness. Scale bars, 40 μm . Insets of suprabasal layers (first and second panels) provide a global view of flat-mounted corneas (scale bars, 500 μm). Inset (third panel) shows cells with multi-lobed nuclei within the corneal stroma directly beneath the wound bed, indicative of neutrophils (scale bar, 10 μm). Nuclei were counterstained with Hoechst (blue). See also Table S1.

(C) Immunofluorescence for K12 (green), K13 (green), and K8/18 (green) in the central cornea 4 weeks post wounding ($n = 3/\text{group}$). Hatched white lines demarcate the epithelial basement membrane. Nuclei are counterstained with DAPI (blue). Scale bars, 20 μm .

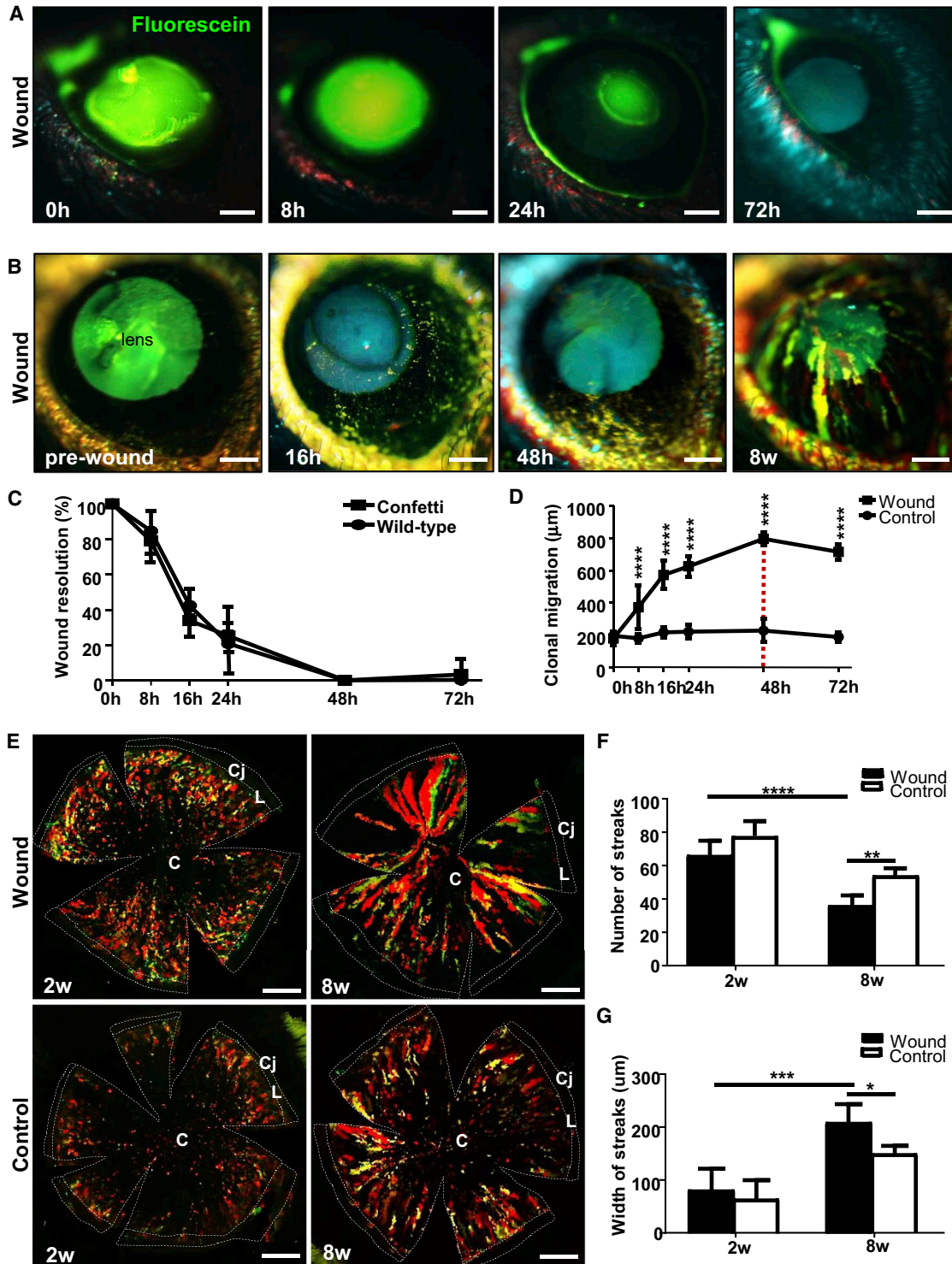


Figure 2. Accelerated Re-epithelialization by K14⁺ Limbal Progenitor-Derived Clones

(A) *In vivo* staining with sodium fluorescein (green) post injury in Confetti corneas (n = 6/group). Scale bars, 400 µm.
 (B) Long-term intra-vital monitoring Confetti clones after injury (n = 6/group). The intraocular lens autofluoresces (blue-green hue). Scale bars, 400 µm.

(legend continued on next page)



627.0 ± 63.4 μm, and 797.6 ± 40.6 μm after 0, 8, 16, 24, and 48 hr, respectively (Figure 2D). In contrast, they were relatively stationary over the same time course in the contralateral control eye, traveling at a rate of 0.53 ± 0.52 μm/hr (p = 0.015), meaning cells in the injured eye moved 37.7-fold faster than under steady state (Figure 2D). Confocal microscopy on flat-mounted corneas provided a higher-resolution perspective of clonal dynamics in wounded and uninjured Confetti corneas (Figure 2E). There was no statistically significant difference in the number of multi-colored clonal streaks at 2 weeks post wounding compared with steady state (67.6 ± 6.2 versus 76.8 ± 4.6; p = 0.14). However, after 8 weeks there were significantly less in the injured compared with unwounded corneas (36.5 ± 6.2 versus 53.8 ± 4.5; p = 0.0003) (Figures 2E and 2F). Furthermore, streak number was reduced at 8 weeks compared with 2 weeks post wounding (p < 0.0001) (Figure 2F) and broadened from 149.9 ± 43.5 μm to 210.0 ± 75.4 μm (p = 0.044) after 8 weeks (Figure 2G). Notably, clonal dynamics at day 0 was excluded from the analysis due to our inability to accurately discriminate fluorescent streaks from undeveloped multi-colored patches. There were few TUNEL⁺ cells detected during wound healing (not shown), and there was no difference compared with steady state (Richardson et al., 2017), suggesting that streak loss was not due to elevated apoptosis. Previous studies showed that loss of limbal clones, concomitant with their widening and/or merging, is suggestive of either increased symmetric division or an accelerated rate of symmetric/asymmetric division after trauma (Klein and Simons, 2011; Richardson et al., 2017).

Proliferation in the Periphery Drives Centripetal Migration to Expedite Wound Closure

To determine how LSCs partake in corneal wound healing, we assessed basal cell proliferation before (wound I) and just after (wound II) wound closure (Figure 3A) in four randomly selected regions within numerically specified concentric zones (Figure 3B). Irrespective of the time post wounding, BrdU⁺ basal epithelia increased within the peripheral (zone 1) compared with the para-central (zone 3) region (Figure 3C, first and third columns). This contrasted with the uninjured contralateral eye in which there was no significant difference (Figure 3C, sec-

ond and fourth columns). Overall, wounding significantly increased basal limbal epithelial cell proliferation by 3.6-fold at 24 hr (19.2% ± 4.4% versus 5.4% ± 1.8%, p = 0.0016) and 2.4-fold at 28 hr (10.8% ± 2.4% versus 4.5% ± 1.41%, p = 0.0099) post wounding compared with steady state (Figure 3D). Moreover, proliferation between 24 and 28 hr was reduced by 1.8-fold post wounding (p = 0.0439) (Figure 3D), indicating that peripheral replication attenuated once the defect sealed.

Corneal Epithelial Wound Closure by Basal Cell Migration

To determine which cells contribute to corneal epithelial wound closure, we examined their phenotype at 0 hr and 24 hr post wounding (Figure 4). At 0 hr post injury, corneal-specific K12 expression was displayed throughout the intact peripheral corneal epithelium, and K14 was restricted to the limbus (Figure 4A, first row, left panel and second row; i and iii). However, K14 was highly expressed within the layer of epithelial cells that covered the defect at 24 hr post injury (Figure 4A, first row, right panel and third row; iv, v, and vi), while K12 was occasionally expressed in superficial cells within the central and peripheral cornea (Figure 4A, first row, right panel and third row; v and vi). This suggests that the regenerated epithelium was derived from K14⁺ basal limbal cells, an observation confirmed in flat-mounted whole corneas, which showed a broader region of K14-stained basal cells at 24 hr post wounding compared with controls (Figure 4B).

Measuring Clonal Displacement with Spatial-Temporal Vector Flow Maps

To accurately map the spatial-temporal dynamics of K14⁺ cells within clones during wound closure, we developed a method to maintain and image corneas in short-term organ culture, after which quantitative STICS analysis was applied. Wounded corneas were imaged by light-sheet microscopy, and cells within K14⁺-Confetti clones migrated in a manner comparable with those in live animals (Video S1). Furthermore, to visualize basal cell migration at a single cell level, we imaged wounded corneas in an *ex vivo* organ culture by confocal microscopy under higher

(C) Percentage wound resolution (i.e., re-epithelialization). by measuring the size of the defect at t = 0 hr compared with other time points. Line graphs represent mean ± SD (n = 3/group/time point). No statistically significant difference was noted between Confetti and WT corneas at any time point (unpaired two-tailed Welch's t test and Sidak's multiple comparisons test).

(D) Clonal displacement in wounded versus unwounded Confetti corneas (mean ± SD, n = 3/group/time point; ****p < 0.0001, Sidak's multiple comparisons test). The red hatched line indicates wound closure.

(E) Confocal images of flat-mounted Confetti corneas at 2 and 8 weeks post 2-mm central injury. Scale bars, 500 μm. C, cornea; L, limbus; Cj, conjunctiva.

(F and G) Streak number (F) and width (G) at 2 and 8 weeks post injury (mean ± SD, n = 3/group/time point). *p < 0.05, **p < 0.01, ***p < 0.001, and ****p < 0.0001, one-way ANOVA with Tukey's multiple comparisons test.

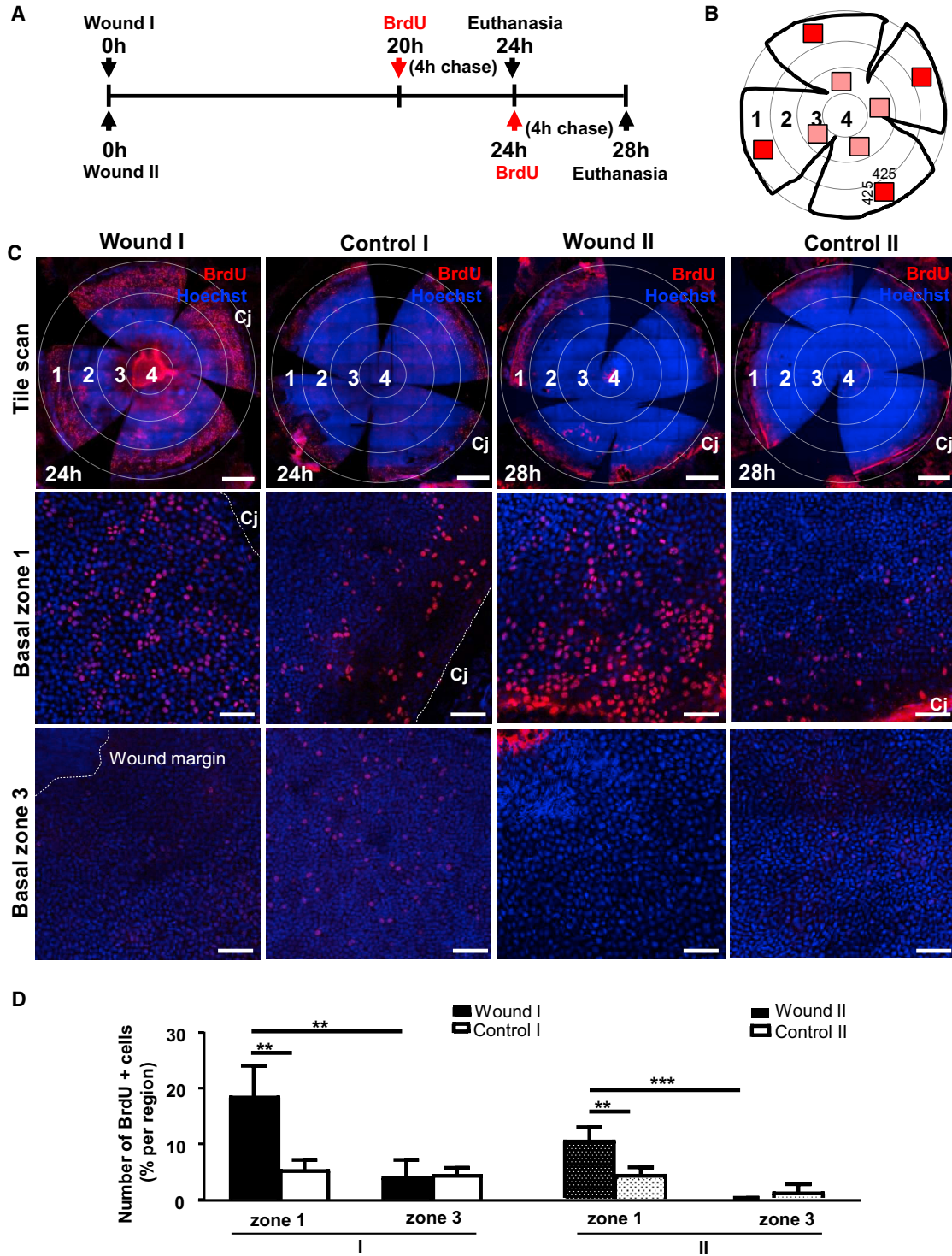


Figure 3. Proliferation of Basal Limbal Epithelia after Inflicting a Central Wound

(A) Schematic of BrdU administration in relation to corneal wounding.

(B) Schematic of a flat-mounted cornea displaying randomly distributed regions (red boxes) that represent areas imaged and analyzed in selected concentric zones that were numbered 1-4.

(legend continued on next page)

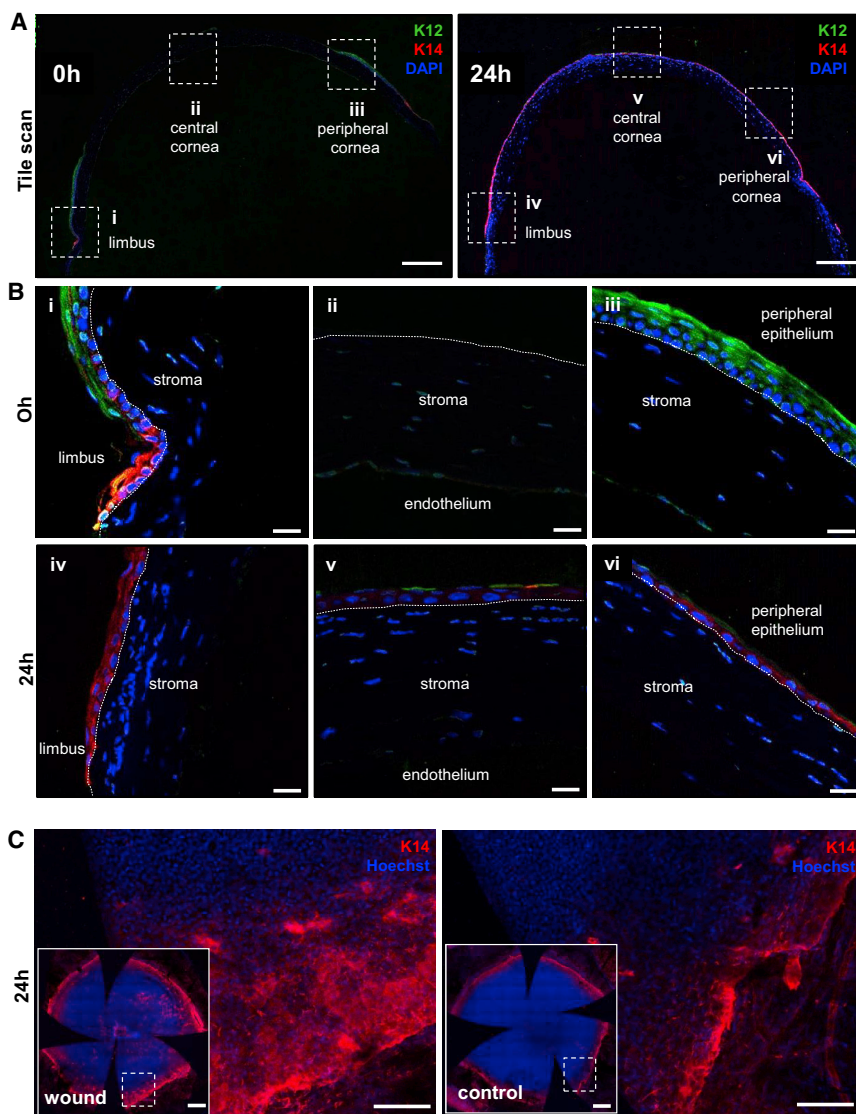


Figure 4. K14 Expression in the Regenerated Corneal Epithelium after Wound Closure

(A) Immunofluorescence was conducted on paraffin-embedded tissue sections ($n = 3/\text{group/time point}$) procured at 0 hr and 24 hr post wounding. Representative corneas were double immunostained for K12 (green) and K14 (red), and counterstained with DAPI (blue). Images of transverse sections provide a panoramic view of the staining across the entire cornea. Scale bars, 200 μm .

(B) Images are magnified views of the region encompassed by the hatched boxes in (A), which focus on the limbal transition zone (i and iv), as well as the central (ii and v) and peripheral (iii and vi) cornea. Hatched white lines demarcate the epithelial basement membrane. Scale bars, 20 μm .

(C) Representative images of whole-mounted corneas displaying K14 expression in limbal/peripheral zone. Insets in each panel provide a global appreciation of the entire cornea ($n = 3/\text{group}$). Specimens were counterstained with Hoechst (blue) to highlight cell nuclei. Scale bars, 100 μm and 500 μm (insets).

magnification (Video S2). Epithelial cells located in and around the wound edge became elongated and moved into the defective area to form a monolayer; these observations certainly align with our *in vivo* results (Figures 1 and 2; Table S1), and suggests that moving cells were likely basal epithelia as indicated by our phenotypic analyses (Figure 4).

At 8 and 36 hr post injury, the direction and velocity of clonal migration was calculated and displayed as vector flow maps (Figure 5A). This analysis indicated that although groups of cells within clones move in a multi-directional

manner (Figure 5A, insets), the overall motion was centripetal (Video S3). Upon closer inspection, clones traveled faster from the limbal margin after 8 hr compared with 36 hr post wounding (Figure 5A). As wounds resolved, clones gradually decelerated from $49.0 \pm 23.4 \mu\text{m/hr}$ at approximately 14 hr to $15.2 \pm 4.9 \mu\text{m/hr}$ from the periphery at 36 hr (Figure 5B) while little or no migration was observed in control eyes. The data are displayed as a spectrum of histograms ranging from light blue (earliest time point of 0 hr) to dark blue (latest time point of 48 hr); the height of each represents the speed of movement.

(C) Confocal images of wounded and control corneas stained for BrdU (red) and counterstained with Hoechst (blue). Scale bars, 500 μm (upper panels) and 100 μm (middle and lower panels). Cj, conjunctiva.

(D) Percentage BrdU⁺ basal epithelial cells between zone 1 (limbal) and zone 3 (para-central), comparing wounded with control corneas (mean \pm SD, $n = 3/\text{group/time point}$; ** $p < 0.01$ and *** $p < 0.001$, two-way ANOVA with a Turkey's multiple comparisons test).

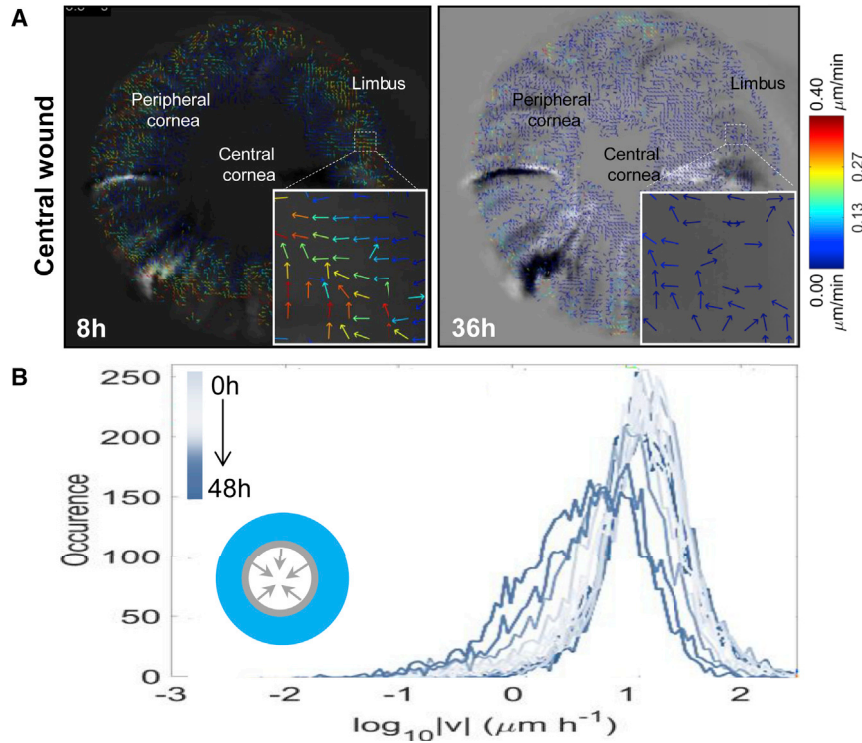


Figure 5. Velocity of Migrating Clones during Ex Vivo Wound Healing Measured by Quantitative STICS Analysis

(A) Eyes from Confetti mice ($n = 3/\text{group}$) were enucleated immediately post wounding, placed in organ culture, and imaged by light-sheet microscopy every 2 hr for 48 hr. Vector flow maps represent cell migration and direction of clone movement from images taken at 8 hr and 36 hr. Insets show the multi-directional movement of groups of cells within a clone, depicted as colored arrows; associated with these images is a heatmap that acts as a speed gauge.

(B) STICS was applied on a time series of 2D maximum-intensity projections of 3D image stacks. The speed of peripherally located clones every 2 hr for a representative cornea is displayed by colored histogram (from light to dark blue). The inset is a schematic representation of the wound, with arrows indicating the direction of closure. See also [Video S3](#).

Dynamics of Corneal Epithelial Wound Healing through Computational Modeling

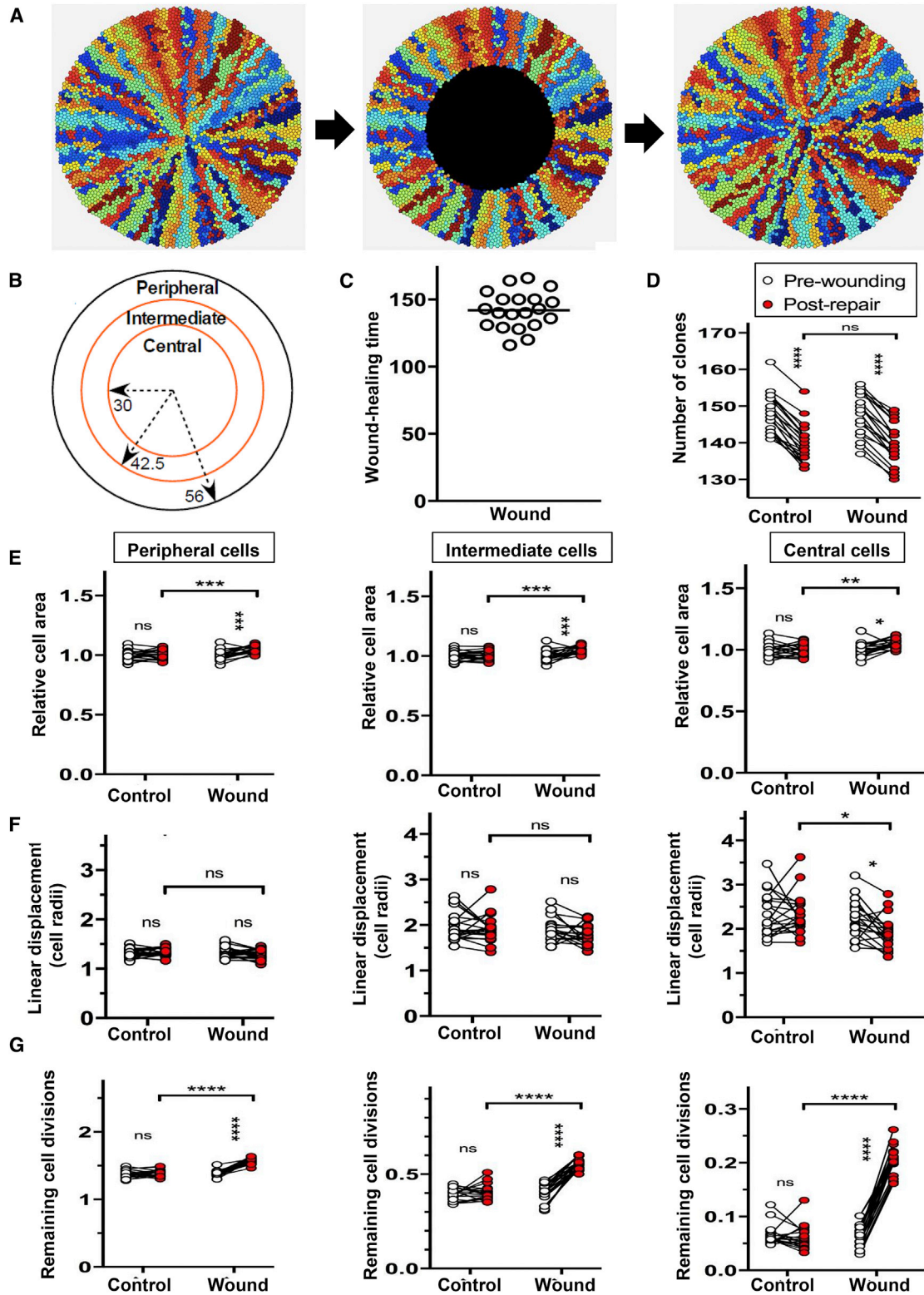
Using animal and computational modeling, we previously showed that population density-driven pressure is sufficient to promote centripetal clonal migration during homeostasis (Lobo et al., 2016; Richardson et al., 2017). To determine whether a similar mechanism plays a role in wound healing, we adapted our mathematical model to incorporate an epithelial injury (Figure 6). Wounds were simulated by replacing cells in the intermediate and central zones, respectively, with “blank” cells (Figures 6A and 6B), which offer minimal resistance to the movement of adjacent epithelia (see [Experimental Procedures](#)). Simulated corneas completely healed the wound within 200 time steps (Figure 6C and [Video S4](#)), and there was no difference in the number of clones between wounded and control, or pre-wounding and post repair (Figure 6D). At the end of the healing process, cell size significantly increased in the peripheral, intermediate, and central zones (Figure 6E and [Table S2](#)); results that agreed with our *in vivo* observations (Figure 1 and [Table S1](#)).

The computational model was also used to examine the effects of wounding on the organization of the corneal epithelium. We quantified the mean linear displacement (Lobo et al., 2016) a measure of clonal dispersion, and found that clones were slightly more cohesive in the peripheral and intermediate zones, consistent with the steeper population density pressure gradient drawing cells

faster through these zones toward the central cornea (Figure 6F). In addition, cell division was high in peripheral cells and gradually decreased in intermediate and central cells (Figure 6G). Thus, while not ruling out a role for signaling molecules released by inflammatory other cells to enhance the epithelial wound-healing response, population pressure seems sufficient to mediate many changes in epithelial behavior that accompany the process of wound healing.

DISCUSSION

Herein we describe the contribution of $K14^+$ -Confetti precursor cells and their progeny to corneal epithelial repair using real-time visual monitoring in live mice. After wounding, centripetal migration of limbal-derived clones was accelerated, and this coincided with elevated mitosis at the periphery. Our intra-vital analysis was supported by data collated from *ex vivo* organ-cultured corneas, an advantageous system because clonal dynamics could be visualized and rendered with high-resolution microscopy and robust image analysis tools. Using this model system, we also provide direct evidence that basal limbal epithelia are the predominant cells involved in the initial phase of injury repair. These cells seem to stream along the basement membrane in a centripetal manner, most likely propelled by population pressure that arises from



(legend on next page)



heightened proliferation in and around the LESC niche upon injury, an observation supported by computational modeling.

It is generally accepted that LESC undergo asymmetric division as a means of maintaining corneal tissue mass. In this scenario, two daughters are produced, including one that remains within the SC pool and the other (a TAC) that leaves the niche, ascending through the epithelial layers before being sloughed from the ocular surface (Di Girolamo, 2015; Richardson et al., 2016, 2017). However, it is likely that a proportion of divisions are symmetric, whereby both daughters either remain or are evicted from the repository (Lamprecht, 1987, 1990; Beebe and Masters, 1996; Castro-Muñozledo and Gómez-Flores, 2011). We recently affirmed this notion through mathematical modeling (Lobo et al., 2016) and via aging experiments in which K14⁺-Confetti clones either disappeared from the trace and/or became broader with time (Richardson et al., 2017). Herein we observed an accentuated clonal pattern (Figure 2E), concordant with spokes widening, especially so at 8 weeks post injury (Figures 2E–2G), a result that aligns with the concept of neutral evolutionary drift (Doupé et al., 2012). A limitation of our study was that gender was not factored into the experimental paradigm and may have influenced some of the readouts. Certainly, there have been several reports of sex differences in relation to corneal wound healing that could be hormonally regulated (Krishnan et al., 2012; Wang et al., 2012). Notably, most aspects of our *in silico* model (Figure 6) recapitulated observations made *in vivo*, with the exception that there was no statistically significant difference in clone number between wounded and control corneas. This suggests that the model may not be capturing clone loss or that the time and space restrictions placed upon the model preclude the manifestation of this phenomenon.

During the initial 24 hr post wounding, epithelial movement (without proliferation) proceeded adjacent to the wound edge (Figures 2 and 3; Videos S1, S2, S3, and S4) while in the periphery, cell replication predominated (Figure 3C). These data support our proposition that increased limbal population pressure is the principal driving force that propels K14⁺ basal cells toward the wound bed to seal the defect (Figure 4 and Video S2). The speed at which basal cells move into the injury site suggests that adhesive connection between these cells and the immature basement membrane are weak and/or diminished; alternatively, secretion of matrix metalloproteinases by these cells would render them more “fluid” (Aragona et al., 2017). In future studies we would like to define the molecular signature of stationary limbal epithelia compared to migratory cells at the wound margin. Certainly, K14 was found to be one of nine upregulated genes in moving rat epithelia after cornea wounding (Yu et al., 1995). In agreement with this study and our K14⁺ migratory cells, Chung et al. (1995) identified the steady-state expression of α -enolase in basal limbal epithelia. After creating a debridement injury in rabbit corneas (like the one our mice endured), the first cells to migrate into the wound were flat, elongated, α -enolase⁺ epithelia thought to be displaced from the intact limbal zone. Furthermore, by 4 weeks post wounding α -enolase expression regressed from the central epithelia, and this was concomitant with basal cells becoming cuboidal to coincide with maturation and re-stratification. Once the defect is covered by a monolayer of epithelia (Figures 1 and 4), suprabasal cells located around the wound edge can crawl over newly migrated basal cells. Alternatively, basal cells themselves could differentiate into K12⁺ wing cells (Figures 4 and 7A–7D) to restore epithelial hierarchy. Notably, our results are incompatible with long-standing models of epithelial wound healing in either the

Figure 6. Computational Modeling to Investigate the Effect of Wounding on the Composition and Structure of the Repaired Corneal Epithelium

- (A) Examples of simulated corneas before and during wounding, and immediately after complete wound repair (left to right).
(B) Wounds equivalent in area were made by removing epithelial cells from the central zone within 30 cell radii of the center of the cornea. Cell properties were measured in these regions and in the peripheral zone.
(C) The wound was completely repaired in less than 200 time steps.
(D) The number of clones was counted before wounding and after repair.
(E) Cell size was measured for all cells in each zone before and after wounding, and immediately after healing was complete or, in the case of unwounded corneas, at $t = 2,300$ (“pre-wounding”) and $t = 2,500$ (“post wounding”). Cell size was adjusted for differences in pre-wounding size, which varied within the three zones. The mean cell area was plotted for each cornea in the peripheral (left), intermediate (middle), and central (right) zone.
(F) The mean linear displacement, a measure of clonal dispersion, was determined for all cells within the peripheral (left), intermediate (middle), and central (right) zone in corneas subjected to a wound, as indicated below the x axis.
(G) The number of remaining cell divisions of the TACs in corneas was determined for all cells in the peripheral (left), intermediate (middle), and central (right) zone in corneas subjected to a wound, as indicated below the x axis.
Data represent mean \pm SD, $n = 20$ /group; * $p < 0.05$, *** $p < 0.001$, **** $p < 0.0001$, ns = $p > 0.05$ by repeated-measures (2,300-time unit) one-way ANOVA with Sidak’s multiple comparisons correction. See also Video S4.

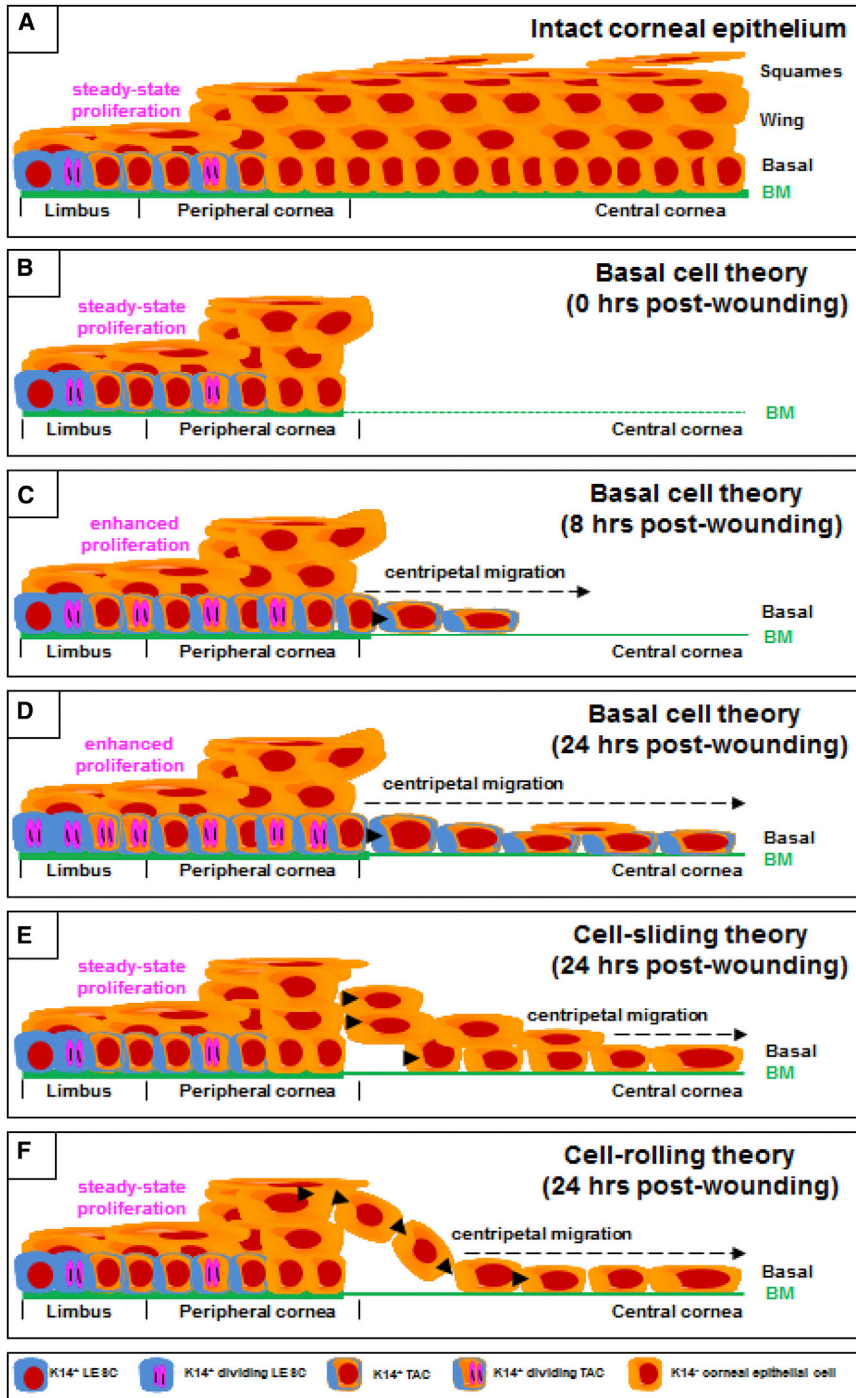


Figure 7. Basal Cell Migration: A Hypothesis for the Early Phase of Re-epithelialization

(A) Under homeostasis the multi-layered squamous epithelium of the mammalian cornea is maintained by slow-cycling, self-sustaining, $K14^+$ LESC located in the limbus.

(B) A mechanical debridement injury removes the epithelium and basement membrane (BM) within a confined region ($t = 0$ hr).

(C and D) The basal cell migration hypothesis. Peripherally located $K14^+$ LESC are activated to proliferate, forcing generations of newly propagated $K14^+$ basal TAC into the wound bed, during which they synthesize an immature BM (solid green line) over the first 8 hr (C) and 24 hr (D). See also Figures 1, 2, 3, and 4; Video S2.

(E) Our basal cell migration hypothesis challenges the “sliding-cell” theory in which epithelia surrounding the wound progressively move into the debrided zone as a block or sheet of cells.

(F) Our basal cell migration hypothesis also challenges the “cell-rolling” proposition whereby suprabasal epithelia role over leading-edge basal cells to form new leader cells.

skin or cornea, which include the “cell-sliding” model, in which epithelial cells move into the wound as a sheet (Figure 7E), and the “cell-rolling” model (also known as the “leap-frog” model), in which suprabasal cells roll over leading-edge cells to become new basal cells (Figure 7F) (Crosson et al., 1986; Danjo and Gipson, 2002; Kuwabara et al., 1976). Our observations are more in line with recent

studies conducted in skin, which demonstrated $K14^+$ basal keratinocytes moving into central cutaneous wounds, behind which are concentric regions of proliferation (Park et al., 2017; Safferling et al., 2013). Furthermore, if superficial $K14^-/K12^+$ corneal epithelia are the first cells arriving in the wound bed, they would likely require ample replicative activity to contribute to vertical epithelial



restoration; this could occur if they had the ability to dedifferentiate (Nasser et al., 2018).

Finally, we employed STICS to quantify the dynamics of corneal epithelial cells during wound healing in an *ex vivo* setting. The advantage of STICS over manually measuring cell migration is that it is readily automated, and vector speeds can be extracted from an image for every spatial and temporal region of data acquired. The inherent computational simplicity of this approach makes it a versatile tool for measuring the dynamics of molecular complexes, for example organelles (Ashdown et al., 2017; Meddens et al., 2016; Toplak et al., 2012) and cells in the context of migration (Tanner et al., 2009). Since this method does not require segmentation and detection of single cells but relies on measuring pixel intensity fluctuations, it is more adaptable to scenarios whereby migrating objects change size and shape over time. It is therefore a preferable choice in complex processes such as during wound healing (Figure 5; Videos S1 and S3). However, STICS is currently limited to 2D mapping, and applying this system on *in vivo* data imposes technical and ethical barriers that must be overcome, such as the frequency of sampling and the inherent challenges of intra-vital imaging (i.e., limited ketamine dosing and animal movement under anesthesia). In the future, we will extend these investigations to include a full 3D plus time vector mapping of cell migration, allowing us to visualize cell movement in all epithelial layers during each phase of wound healing.

In this study, we visualized the deployment of K14⁺-derived limbal epithelial cells into the wound bed and propose the “basal cell migration” theory, which was substantiated in an organ-culture system and with computational modeling. Our results indicate that there is cellular activity beyond what occurs in the immediate vicinity of the wound, and to this end we provide evidence that heightened proliferative population pressure from the limbal perimeter is the main driver of centripetal epithelial cell movement upon injury.

EXPERIMENTAL PROCEDURES

Mice

K14CreER^{T2}-Confetti (n = 28 eyes) and age-matched WT C57BL/6 (n = 63 eyes) male and female mice were housed under pathogen-free conditions and fed standard chow (Gordon's Specialty Feeds, Yanderra, Australia). All studies were conducted in accordance with the Australian Code of Practice for the Care and Use of Animals for Scientific Purposes. All procedures were approved by the UNSW Animal Care and Ethics Committee (Approval No. 17/81A).

Six-week-old male and female transgenic mice (heterozygous for K14CreER^{T2} and homozygous for Confetti) were injected intraperitoneally with 50 µg/g body weight of tamoxifen (Sigma-Aldrich, St Louis, MO) dissolved in 10% ethanol and 90% olive oil

(Sigma-Aldrich) over 3 consecutive days. Mice were used at 1 or 24 weeks post tamoxifen injection, rendering them 7–30 weeks of age for experimentation. This facilitated the development of a multi-colored fluorescent streaking pattern arising from marginally located K14⁺ LESC (Di Girolamo et al., 2015; Lobo et al., 2016; Richardson et al., 2017).

Inducing, Monitoring, and Assessing Corneal Epithelial Debridement Wounds

Mice were anesthetized by an intraperitoneal injection of 100 µg/g ketamine (Provet, Eastern Creek, NSW, Australia) and 10 µg/g xylazine (Sigma-Aldrich), after which they were placed under an OPMI pico (Carl Zeiss, Jena, Germany) surgical microscope. Epithelial debridement was performed with an Algerbrush II (Katena Products, Denville, NJ) as previously described (Chan and Werb, 2015). In brief, a central corneal debridement injury was created by marking a limbal-sparing central circle using a 2-mm trephine (KAI Medical, Solingen, Germany), then removing the epithelium using an Algerbrush II attached to a 1-mm burr. After wounding, the right eye was rinsed with saline to remove cell debris; the left eye was uninjured and acted as the internal control. Saline was instilled in both eyes to maintain hydration while mice recovered. Eyes were monitored by fluorescence microscopy (3i VIVO; Intelligent Imaging Innovations, Denver, CO). Flat-mounted corneas were imaged by confocal fluorescence microscopy (Zeiss LSM 780; Carl Zeiss). Histological and phenotypical assessments were performed with PAS and immunofluorescence staining (see details in Supplemental Information: Histological Assessment, Immunofluorescence, Measuring Clonal Migration and Wound Closure by Intra-vital Microscopy and Confocal Microscopy).

Monitoring Corneal Wound Resolution in Organ Culture

Confetti mice were wounded as described above. The animals were euthanized and their eyes immediately enucleated. Paired (wounded and intact) globes were embedded in sterile 1.5% agarose and placed within the microscope's imaging/incubation chamber, set to 37°C and 5% CO₂ prior to immersion in defined keratinocyte serum-free medium (Gibco, Fremont, CA) containing 50 nM recombinant human epidermal growth factor (Peprotech, Rocky Hill, NJ), 500 nM cholera toxin (List Biological Labs, Campbell, CA) and 100 U/mL penicillin-streptomycin (Gibco). Eyes were imaged every 2 hr over 48 hr by light-sheet microscopy (Zeiss Lightsheet Z.1) using a 5×/0.16 detection lens and 5×/0.1 illumination lens as described above.

Cell Proliferation by BrdU Incorporation

To determine the level of proliferation, we wounded WT mice (as described above) and injected them intraperitoneally with BrdU (100 µg/g body weight) (Sigma-Aldrich) at 20 or 24 hr post wounding. After 4 hr, mice were euthanized, and their eyes enucleated and fixed in 4% paraformaldehyde overnight at 4°C. Corneas were dissected and stained for BrdU as previously described (Pajoohesh-Ganji et al., 2006; Richardson et al., 2017). In brief, corneas were treated with 2 N HCl for 20 min at room temperature, washed four times (5 min each)



in PBS at room temperature, blocked in 20% goat serum diluted in PBS containing 2% BSA and 0.1% Triton X-100 (PBS-BT) overnight at 4°C, then reacted with a rat anti-BrdU antibody (5 µg/mL; ab6326, Abcam) in PBS-BT for 48 hr at 4°C. Corneas were washed thrice (20 min each) in PBS-BT at room temperature, incubated with a goat anti-rat Alexa-Fluor⁶³³-conjugated secondary antibody (5 µg/mL; Life Technologies) at 4°C, counterstained with Hoechst 33342 (1 µg/mL; Life Technologies), and flat-mounted as described above in ProLong Gold anti-fade reagent. To analyze the number of BrdU⁺ basal cells, we randomly selected four regions (425 × 425 µm), each within the limbal margin and central cornea, from confocal scans, then counted BrdU⁺ cells over unlabeled cells and generated a labeling index. A grid with four equally distant concentric rings was drawn over each cornea, and zones numbered accordingly: 1 (limbus), 2 (peripheral cornea), 3 (para-central), and 4 (central). BrdU⁺ basal epithelia within zones 1 and 3 were counted in each of four randomly selected regions that measured 425 × 425 µm in area.

Spatiotemporal Image Correlation Spectroscopy of Clonal Migration in *Ex Vivo* Wounded Corneas

As an alternative and more accurate means of measuring cell movement, spatiotemporal image correlation spectroscopy (STICS) (Ashdown et al., 2017; Meddens et al., 2016; Toplak et al., 2012) was applied on a series of 2D maximum-intensity projections of 3D image stacks that were acquired via light-sheet microscopy at different time points post injury in *ex vivo* organ-cultured murine corneas. The raw data consisted of a temporal sequence (i.e., time point per 2 hr) of z stacks from corneas imaged through a 5×/0.16 detection lens and 5×/0.1 illumination lens as described above (pixel size 2.28 µm) (see details in [Supplemental Information: Spatiotemporal Image Correlation Spectroscopy of Clonal Migration in *Ex Vivo* Wounded Corneas](#)).

Computational Model of Corneal Epithelial Wound Healing

A mathematical model was used to investigate the role that population pressure-driven motility plays in corneal wounding and repair and to compare spatial distributions of clonally related cells in corneas, following cases of no wounding and wounding of the central cornea. It was based on a previous model (Grimm et al., 2010; Lobo et al., 2016), and modified to incorporate regions in which epithelial cells were removed by wounding. This was achieved by substituting a new type of agent, “blank cells,” for the epithelial cells of the wound area. Blank cells exerted less pressure on neighboring cells than epithelial cells. Blank cells were further classified as internal blank cells, which were only adjacent to other blank cells, and edge blank cells, which were adjacent to at least one epithelial cell.

The model space was a circular region representing the corneal epithelium and adjacent limbus, which collectively is in one of three states: a “healthy state,” an “early wounded state,” and a “late wounded state.” The healthy state represents a cornea whose dynamics did not incorporate any wound or any active response to previous wounding. The early wounded state represents a cornea that was undergoing repair, where the key driver

of wound repair was cell movement into the vacant wounded area before the wound approaches closure. The late wounded state represents a cornea that had almost transitioned to the healthy state, where the key component of wound repair was cells coming together spatially, which results in final closure of the wound. LESC s had a 2.5-fold increase in proliferation as a response to wounding, which was sufficient to maintain the epithelium outside of the wound and supply cells for the wounded area. In the early wounded state, epithelial cells more effectively pushed into blank cells than into other cells in the cornea, due to the reduced pressure exerted by blank cells. This produced the preference for cells to move into unoccupied wounded areas of the cornea over competing for space with other cells. Blank cells remained in the cornea and could occupy less of the basal layer, but they were not removed in the early wounded state. The cornea moved from an early wounded state to a late wounded state when there were more edge blank cells than internal blank cells. In the late wounded state, blank cells were removed automatically when the distance between two internal blank cells was less than 0.15 idealized cell radii. At this time they were replaced by a single blank cell whose position takes the value of the average position of the two internal cells being replaced. During the late wounded state, blank cells were also removed stochastically with $p = 0.2$ per blank cell per time step and were not replaced (see details in [Supplemental Information: Overview, Design Concepts, and Details of the Mathematical Model](#)).

Statistical Analysis

Data are presented as mean ± SD (n denotes sample size). Unpaired two-tailed Welch’s t test with unequal variance and ANOVA with Sidak’s or Tukey’s multiple comparisons was used to compare wound closure between WT and Confetti mice, and the velocity of K14⁺ clonal migration, clone number, and streak width between wounded and contralateral control eyes. A p value of <0.05 was considered statistically significant.

SUPPLEMENTAL INFORMATION

Supplemental Information includes Supplemental Experimental Procedures, one figure, two tables, and four videos and can be found with this article online at <https://doi.org/10.1016/j.stemcr.2018.11.014>.

AUTHOR CONTRIBUTIONS

Conceptualization, M.P. and N.D.; Methodology, M.P., A.R., E.P., E.P.L., and S.L.W.; Investigation, M.P., A.R., E.P., and E.P.L.; Writing – Original Draft, M.P. and N.D.; Writing – Review and Editing, M.P., A.R., E.P., E.P.L., R.W., S.L.W., J.G.L., D.W., and N.D.; Funding Acquisition, N.D., D.W., and S.L.W.; Resources, R.W., D.W., and N.D.; Supervision, N.D., D.W., J.G.L., R.W., and S.L.W.

ACKNOWLEDGMENTS

This work was supported by the Australian National Health and Medical Research Council (APP1101078) to N.D., S.L.W., and D.W. The authors thank Richard Francis, Sandra Fok, Iveta Slapevtova, and Fei Shang (Biomedical Imaging Facility, University of



NSW, Sydney, Australia) for their assistance with intra-vital, light-sheet, and confocal imaging and analysis, and assistance with histological sectioning.

Received: September 25, 2018

Revised: November 15, 2018

Accepted: November 16, 2018

Published: December 13, 2018

REFERENCES

- Aragona, M., Dekoninck, S., Rulands, S., Lenglez, S., Mascré, G., Simons, B.D., and Blanpain, C. (2017). Defining stem cell dynamics and migration during wound healing in mouse skin epidermis. *Nat. Commun.* **8**, 14684.
- Ashdown, G.W., Burn, G.L., Williamson, D.J., Pandžić, E., Peters, R., Holden, M., Ewers, H., Shao, L., Wiseman, P.W., and Owen, D.M. (2017). Live-cell super-resolution reveals F-actin and plasma membrane dynamics at the T cell synapse. *Biophys. J.* **112**, 1703–1713.
- Beebe, D.C., and Masters, B.R. (1996). Cell lineage and the differentiation of corneal epithelial cells. *Invest. Ophthalmol. Vis. Sci.* **37**, 1815–1825.
- Buck, R.C. (1985). Measurement of centripetal migration of normal corneal epithelial cells in the mouse. *Invest. Ophthalmol. Vis. Sci.* **26**, 1296–1299.
- Castro-Muñozledo, F., and Gómez-Flores, E. (2011). Challenges to the study of asymmetric cell division in corneal and limbal epithelia. *Exp. Eye Res.* **92**, 4–9.
- Chan, M.F., and Werb, Z. (2015). Animal models of corneal injury. *Bio Protoc.* **5**, e1516.
- Chung, E.-H., DeGregorio, P.G., Wasson, M., and Zieske, J.D. (1995). Epithelial regeneration after limbus-to-limbus debridement. Expression of alpha-enolase in stem and transient amplifying cells. *Invest. Ophthalmol. Vis. Sci.* **36**, 1336–1343.
- Chung, E.H., Hutcheon, A.E., Joyce, N.C., and Zieske, J.D. (1999). Synchronization of the G1/S transition in response to corneal debridement. *Invest. Ophthalmol. Vis. Sci.* **40**, 1952–1958.
- Cotsarelis, G., Cheng, S.-Z., Dong, G., Sun, T.-T., and Lavker, R.M. (1989). Existence of slow-cycling limbal epithelial basal cells that can be preferentially stimulated to proliferate: implications on epithelial stem cells. *Cell* **57**, 201–209.
- Crosson, C., Klyce, S., and Beuerman, R. (1986). Epithelial wound closure in the rabbit cornea. A biphasic process. *Invest. Ophthalmol. Vis. Sci.* **27**, 464–473.
- Danjo, Y., and Gipson, I.K. (2002). Specific transduction of the leading edge cells of migrating epithelia demonstrates that they are replaced during healing. *Exp. Eye Res.* **74**, 199–204.
- Di Girolamo, N. (2015). Moving epithelia: tracking the fate of mammalian limbal epithelial stem cells. *Prog. Retin. Eye Res.* **48**, 203–225.
- Di Girolamo, N., Bobba, S., Raviraj, V., Delic, N., Slapetova, I., Nicovich, P., Halliday, G., Wakefield, D., Whan, R., and Lyons, J. (2015). Tracing the fate of limbal epithelial progenitor cells in the murine cornea. *Stem Cells* **33**, 157–169.
- Doupé, D.P., Alcolea, M.P., Roshan, A., Zhang, G., Klein, A.M., Simons, B.D., and Jones, P.H. (2012). A single progenitor population switches behavior to maintain and repair esophageal epithelium. *Science* **337**, 1091–1093.
- Fujikawa, L., Foster, C., Harrist, T., Lanigan, J., and Colvin, R. (1981). Fibronectin in healing rabbit corneal wounds. *Lab. Invest.* **45**, 120–129.
- Gipson, I.K., and Kiorpes, T.C. (1982). Epithelial sheet movement: protein and glycoprotein synthesis. *Dev. Biol.* **92**, 259–262.
- Grimm, V., Berger, U., DeAngelis, D.L., Polhill, J.G., Giske, J., and Railsback, S.F. (2010). The ODD protocol: a review and first update. *Ecol. Model.* **221**, 2760–2768.
- Huang, A., and Tseng, S. (1991). Corneal epithelial wound healing in the absence of limbal epithelium. *Invest. Ophthalmol. Vis. Sci.* **32**, 96–105.
- Klein, A.M., and Simons, B.D. (2011). Universal patterns of stem cell fate in cycling adult tissues. *Development* **138**, 3103–3111.
- Krishnan, T., Prajna, N.V., Gronert, K., Oldenburg, C.E., Ray, K.J., Keenan, J.D., Lietman, T.M., and Acharya, N.R. (2012). Gender differences in re-epithelialisation time in fungal corneal ulcers. *Br. J. Ophthalmol.* **96**, 137–138.
- Kuwabara, T., Perkins, D.G., and Cogan, D.G. (1976). Sliding of the epithelium in experimental corneal wounds. *Invest. Ophthalmol. Vis. Sci.* **15**, 4–14.
- Lamprecht, J. (1987). Mitosis in the corneal epithelium. A preliminary communication on the coexistence of differential and equivalent cell divisions. *Cell Biol. Int. Rep.* **11**, 449–455.
- Lamprecht, J. (1990). Symmetric and asymmetric cell division in rat corneal epithelium. *Cell Prolif.* **23**, 203–216.
- Lehrer, M.S., Sun, T.-T., and Lavker, R.M. (1998). Strategies of epithelial repair: modulation of stem cell and transit amplifying cell proliferation. *J. Cell Sci.* **111**, 2867–2875.
- Li, Z., Burns, A.R., and Smith, C.W. (2006). Two waves of neutrophil emigration in response to corneal epithelial abrasion: distinct adhesion molecule requirements. *Invest. Ophthalmol. Vis. Sci.* **47**, 1947–1955.
- Lin, Z., He, H., Zhou, T., Liu, X., Wang, Y., He, H., Wu, H., and Liu, Z. (2013). A mouse model of limbal stem cell deficiency induced by topical medication with the preservative benzalkonium chloride. *Invest. Ophthalmol. Vis. Sci.* **54**, 6314–6325.
- Lobo, E.P., Delic, N.C., Richardson, A., Raviraj, V., Halliday, G.M., Di Girolamo, N., Myerscough, M.R., and Lyons, J.G. (2016). Self-organized centripetal movement of corneal epithelium in the absence of external cues. *Nat. Commun.* **7**, 12388.
- Meddens, M.B., Pandzic, E., Slotman, J.A., Guillet, D., Joosten, B., Mennens, S., Paardekooper, L.M., Houtsmuller, A.B., Van Den Dries, K., and Wiseman, P.W. (2016). Actomyosin-dependent dynamic spatial patterns of cytoskeletal components drive mesoscale podosome organization. *Nat. Commun.* **7**, 13127.
- Mort, R.L., Ramaesh, T., Kleinjan, D.A., Morley, S.D., and West, J.D. (2009). Mosaic analysis of stem cell function and wound healing in the mouse corneal epithelium. *BMC Dev. Biol.* **9**, 4.



- Nagasaki, T., and Zhao, J. (2003). Centripetal movement of corneal epithelial cells in the normal adult mouse. *Invest. Ophthalmol. Vis. Sci.* *44*, 558–566.
- Nasser, W., Amitai-Lange, A., Soteriou, D., Hanna, R., Tiosano, B., Fuchs, Y., and Shalom-Feuerstein, R. (2018). Corneal-committed cells restore the stem cell pool and tissue boundary following injury. *Cell Rep.* *22*, 323–331.
- Pajoohesh-Ganji, A., Pal-Ghosh, S., Simmens, S.J., and Stepp, M.A. (2006). Integrins in slow-cycling corneal epithelial cells at the limbus in the mouse. *Stem Cells* *24*, 1075–1086.
- Pajoohesh-Ganji, A., Pal-Ghosh, S., Tadvalkar, G., and Stepp, M.A. (2012). Corneal goblet cells and their niche: implications for corneal stem cell deficiency. *Stem Cells* *30*, 2032–2043.
- Park, S., Gonzalez, D.G., Guirao, B., Boucher, J.D., Cockburn, K., Marsh, E.D., Mesa, K.R., Brown, S., Rompolas, P., and Haberman, A.M. (2017). Tissue-scale coordination of cellular behaviour promotes epidermal wound repair in live mice. *Nat. Cell Biol.* *19*, 155–163.
- Petrescu, M.S., Larry, C.L., Bowden, R.A., Williams, G.W., Gagen, D., Li, Z., Smith, C.W., and Burns, A.R. (2007). Neutrophil interactions with keratocytes during corneal epithelial wound healing: a role for CD18 integrins. *Invest. Ophthalmol. Vis. Sci.* *48*, 5023–5029.
- Ramaesh, T., Ramaesh, K., Leask, R., Springbett, A., Riley, S.C., Dhillon, B., and West, J.D. (2006). Increased apoptosis and abnormal wound-healing responses in the heterozygous Pax6+/- mouse cornea. *Invest. Ophthalmol. Vis. Sci.* *47*, 1911–1917.
- Richardson, A., Lobo, E.P., Delic, N.C., Myerscough, M.R., Guy Lyons, J., Wakefield, D., and Di Girolamo, N. (2017). Keratin-14-positive precursor cells spawn a population of migratory corneal epithelia that maintain tissue mass throughout life. *Stem Cell Reports* *9*, 1081–1096.
- Richardson, A., Wakefield, D., and Di Girolamo, N. (2016). Fate mapping mammalian corneal epithelia. *Ocul. Surf.* *14*, 82–99.
- Safferling, K., Sütterlin, T., Westphal, K., Ernst, C., Breuhahn, K., James, M., Jäger, D., Halama, N., and Grabe, N. (2013). Wound healing revised: a novel reepithelialization mechanism revealed by in vitro and in silico models. *J. Cell Biol.* *203*, 691–709.
- Stepp, M.A., Zieske, J.D., Trinkaus-Randall, V., Kyne, B.M., Pal-Ghosh, S., Tadvalkar, G., and Pajoohesh-Ganji, A. (2014). Wounding the cornea to learn how it heals. *Exp. Eye Res.* *121*, 178–193.
- Tanner, K., Ferris, D.R., Lanzano, L., Mandefro, B., Mantulin, W.W., Gardiner, D.M., Rugg, E.L., and Gratton, E. (2009). Coherent movement of cell layers during wound healing by image correlation spectroscopy. *Biophys. J.* *97*, 2098–2106.
- Thoft, R.A., and Friend, J. (1983). The X, Y, Z hypothesis of corneal epithelial maintenance. *Invest. Ophthalmol. Vis. Sci.* *24*, 1442–1443.
- Toplak, T., Pandzic, E., Chen, L., Vicente-Manzanares, M., Horwitz, A.R., and Wiseman, P.W. (2012). STICCS reveals matrix-dependent adhesion slipping and gripping in migrating cells. *Biophys. J.* *103*, 1672–1682.
- Wang, S.B., Hu, K.M., Seamon, K.J., Mani, V., Chen, Y., and Gronert, K. (2012). Estrogen negatively regulates epithelial wound healing and protective lipid mediator circuits in the cornea. *FASEB J.* *26*, 1506–1516.
- Yu, F.X., Gipson, I.K., and Guo, Y. (1995). Differential gene expression in healing rat corneal epithelium. *Invest. Ophthalmol. Vis. Sci.* *36*, 1997–2007.
- Zhao, M., Song, B., Pu, J., Forrester, J.V., and McCaig, C.D. (2003). Direct visualization of a stratified epithelium reveals that wounds heal by unified sliding of cell sheets. *FASEB J.* *17*, 397–406.
- Zieske, J., and Gipson, I. (1986). Protein synthesis during corneal epithelial wound healing. *Invest. Ophthalmol. Vis. Sci.* *27*, 1–7.

Stem Cell Reports, Volume 12

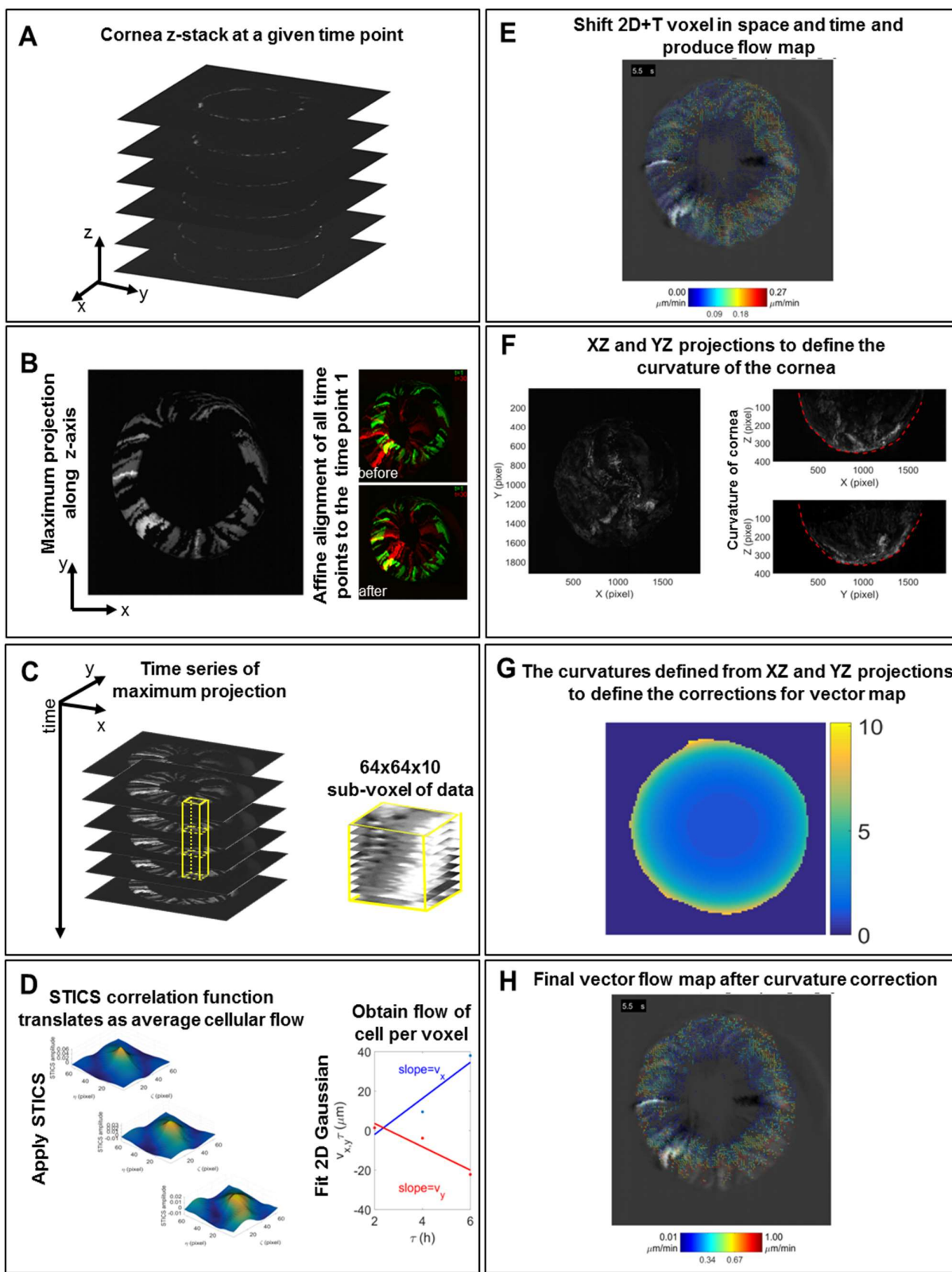
Supplemental Information

**Visualizing the Contribution of Keratin-14⁺ Limbal Epithelial Precursors
in Corneal Wound Healing**

Mijeong Park, Alexander Richardson, Elvis Pandzic, Erwin P. Lobo, Renee Whan, Stephanie L. Watson, J. Guy Lyons, Denis Wakefield, and Nick Di Girolamo

1 Supplementary Figures and Text

2 Figure S1



3
4
5

1 **Supplementary Figure Legend**

2 **Figure S1: Spatio-Temporal Image Correlation Spectroscopy (STICS) pipeline**

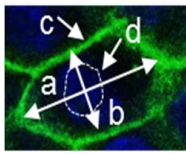
3 (A) Cornea Z-stacks were acquired every 2 hrs for 48 hrs from *ex vivo* organ-cultured corneas using light-sheet
 4 microscopy. (B) The maximum intensity projection (MIP) was calculated along the Z-axis for every time point and
 5 MIPs from all four channels were merged to produce a single gray-scale time series in the X-Y plane. Every time point
 6 in the series was then aligned to the first time point. (C) STICS was applied on the registered time series of MIP; 64×64
 7 pixels by 10 frames. (D) STICS correlation function was calculated using a fast fourier transform, and fitted by a 2D
 8 Gaussian function at each time lag, and peak positions were further linear-fitted to extract the flow vector (velocities in
 9 X and Y directions; v_x, v_y) for each voxel. (E) An example of full velocity vector map for an early time point. Blue to
 10 red arrows indicate increase in velocity. (F) The cornea curvature is measured on X-Z and Y-Z projections of Z-stacks.
 11 (G) The correction vector map is calculated from the curvature traces. (H) Correction map is multiplied to correct the
 12 velocity map from (E) to account for the difference in clonal displacement along corneal curvature.

13

14 **Supplementary Tables**

15

16 **Table S1. Basal epithelial cell dimension and epithelial thickness adjacent the wound margin in 2 mm central**
 17 **wounds, related to Figure 1B.**

	Size of cells (axis; μm)		Perimeter (μm)		Cell density (425×425 μm)	Epithelial thickness (μm)
	Maximum (a)	Minimum (b)	Cell (c)	Nuclei (d)		
Wound	15.5 ± 2.0	10.3 ± 0.6	46.2 ± 5.1	28.3 ± 2.4	1608.3 ± 444.6	12.0 ± 0.7
Control	11.5 ± 1.1	7.1 ± 0.4	34.3 ± 2.6	25.1 ± 1.9	3131.3 ± 593.2	18.2 ± 0.8
p value	0.0198 (*)	0.0003 (***)	0.0113 (*)	0.15 (ns)	0.0117 (*)	<0.0001 (****)

18 *Seven-wk-old WT mice had their right corneal epithelium debrided to create a 2 mm central wound. Average*
 19 *measurement of each parameter was obtained from PFA-fixed and flat-mounted phalloidin-stained corneas at 16 hrs*
 20 *post-injury by scanning confocal microscopy. Data represent mean ± SD, n=4/group, * p <0.05, *** p < 0.001, **** p <*
 21 *0.0001, ns = p >0.05 using an unpaired two-tailed Welch's t-test.*

22

23

24

1 **Table S2. Average size of basal epithelial cells from simulated corneas, related to Figure 6 and Video 4.**

	Relative to cell area		
	Peripheral cells	Intermediate cells	Central cells
Wound	1.04 ± 0.03	1.05 ± 0.03	1.04 ± 0.04
Control	1.0 ± 0.04	1.0 ± 0.05	1.0 ± 0.06
p value	0.0007 (***)	0.0006 (***)	0.0116 (*)

2 *The average size of the basal cells was significantly increased in the central region compared to peripheral and*
3 *intermediate zones Data represent mean ± SD, n=20/group, *p<0.05, ***p< 0.001, ****p< 0.0001 by repeated*
4 *measures (2300 time unit) one-way ANOVA with Sidak multiple comparisons correction.*

5

6 **Supplementary Experimental Procedures**

7 **Histological assessment**

8 Mice were sacrificed by cervical dislocation at specific time points post-wounding. Eyes were enucleated, fixed in 10%
9 neutral buffered formalin overnight at room temperature (RT), then placed in 70% ethanol. Corneas were procured from
10 intact globes and bisected prior to embedding in agarose then paraffin; this ensured correct orientation relative to the
11 wound. Tissue sections (4 µm) were cut, dewaxed and rehydrated prior to staining with hematoxylin and eosin (H&E)
12 or periodic acid Schiff (PAS). They were mounted in DPX mounting medium (Sigma-Aldrich), observed under a BX51
13 light microscope (Olympus, Center Valley, PA), imaged on a digital camera (DP73; Olympus) and processed using
14 CellSens® (Olympus).

15

16 **Immunofluorescence**

17 To confirm the phenotype of the regenerated epithelium, mice were euthanized at specific time points post-wounding,
18 eyes were enucleated and fixed in 10% neutral buffered formalin, and corneas dissected and paraffin-embedded.
19 Antigen retrieval was performed by placing slides in Target Retrieval™ (Dako, Glostrup, Denmark) solution for 5 min
20 at 110°C in a NxGen® Decloaking Chamber (Biocare Medical, Pacheco, CA). Sections were equilibrated in Tris-
21 buffered saline (TBS, pH 7.6) then blocked in 20% goat or rabbit serum diluted in TBS containing 2% bovine serum
22 albumin (TBS-B) (Sigma-Aldrich) for 1 hr at RT. Next, they were incubated for 2 hrs at RT with a pre-determined
23 concentration of primary antibody (Ab) including goat anti-K12 (2 µg/ml; sc-17101; Santa Cruz, Dallas, TX), goat anti-
24 K13 (2 µg/ml; sc-31703; Santa Cruz), rabbit anti-K14 (1 µg/ml; GTX104124; GenTex, San Antonio, TX) and rat anti-
25 K8/18 (2 µg/ml; TROMA-I; DSHB, Iowa City, IA) in TBS-B. Abs to rabbit (Santa Cruz), goat (Santa Cruz) and rat
26 (Life Technologies, Carlsbad, CA) IgG were used as reagent negative controls. Sections were flooded with TBS to

1 remove unbound Abs, then reacted with Alexa-Fluor⁴⁸⁸-conjugated rabbit anti-goat, Alexa-Fluor⁶⁴⁷-conjugated chicken
2 anti-rabbit or Alexa-Fluor⁴⁸⁸-conjugated goat anti-rat secondary Abs (Life Technologies) in TBS-B at a final
3 concentration of 5 µg/ml for 45 mins at RT. Sections were mounted in ProLong Gold[®] anti-fade containing DAPI (Life
4 Technologies), viewed under a BX51 fluorescence microscope (Olympus), images taken on a DP73 digital camera
5 (Olympus) and processed using CellSens[®] (Olympus). For K12/K14 double-staining, images were acquired on a Zeiss
6 780 confocal microscope (Carl Zeiss).

7

8 **Measuring clonal migration and wound closure by intra-vital microscopy**

9 Anaesthetized Confetti and WT mice were placed under a 3i VIVO[™] fluorescence microscope (Intelligent Imaging
10 Innovations, Denver, CO), and wide-field images acquired using 4 filters compatible for CFP, GFP, YFP and RFP to
11 record the status of the ocular surface prior to wounding; CFP 458 nm excitation, 464-495 nm emission; GFP 488 nm
12 excitation, 497-510 nm emission; YFP 514 nm excitation, 517-540 nm emission; RFP 561 nm excitation, 575-654 nm
13 emission. A droplet (25 µl) of 0.1% sodium fluorescein (Minims, iNova Pharmaceuticals, Sydney, Australia) was
14 instilled for 5 sec, each eye was rinsed with 5 ml of PBS, then corneas imaged again. At selective time points, corneas
15 were assessed by intravital microscopy using a 2.5×/0.085 detection lens, images were taken and processed using
16 SlideBook v.6 (3i Intelligent Imaging Innovations, <https://www.intelligent-imaging.com>) and ImageJ software (NIH,
17 <https://imagej.nih.gov/ij>) (Abràmoff et al., 2004; Cruzat et al., 2011). Wound closure rate was estimated from
18 measurements taken after applying fluorescein. Clonal migration in Confetti mice was estimated by measuring the
19 length of 5 or more limbal-originating streaks of each color over time, and the rate expressed as µm/hr (Di Girolamo et
20 al., 2015; Lobo et al., 2016; Richardson et al., 2017). At least 3 mice were used per group/time point. Due to the
21 elevated K14⁺ clonal migration during wound-healing and due to the limited amount of ketamine animals could endure
22 over this period, two groups of mice were established in which the monitoring period was offset. Live Confetti mice in
23 Group 1 were inspected at 0 hrs, 8 hrs, 24 hrs and 72 hrs, and those in Group 2 at 0 hrs, 16 hrs, 48 hrs and 72 hrs post-
24 injury.

25

26 **Confocal microscopy**

27 Confetti transgenic mice were euthanized at designated time points post-wounding, eyes were enucleated, fixed in 4%
28 paraformaldehyde overnight at 4°C, then placed in PBS prior to experimentation. Corneas were procured, extraneous
29 tissues (lens, iris, retina and ocular muscles) removed and imaged by confocal fluorescence microscopy (Zeiss LSM
30 780; Carl Zeiss) with a 20×/0.8 or 100×/1.4 detection lens. The four fluorescent protein signatures were collected
31 sequentially as follows; CFP 458 nm excitation, 455-499 nm emission; GFP 488 nm excitation, 490-508 nm emission;
32 YFP 514 nm excitation, 517-544 nm emission; RFP 561 nm excitation, 579-659 nm emission. Four relaxing radial

1 incisions were made on the corneas to facilitate flat-mounting. Corneas were placed epithelial side-down on glass slides,
2 mounted in ProLong Gold[®] anti-fade reagent containing DAPI (Life Technologies), weighted overnight to facilitate
3 flattening, and imaged using a Zeiss 780 confocal microscope (Carl Zeiss). To capture the entire sample, 121 frames
4 were merged into a single 11×11 tiled image. Z-stack images were collected, merged using a maximum intensity
5 projection with Zen (Carl Zeiss), then analyzed with ImageJ software. The number of fluorescent stripes was
6 determined by manually counting each as they emerged from limbal margin. Clone width at the periphery was
7 estimated (using a scale bar as a reference) from at least 10 fluorescent streaks comprising YFP and RFP (Richardson et
8 al., 2017).

9

10 **Spatio-Temporal Image Correlation Spectroscopy of clonal migration in *ex vivo* wounded corneas**

11 As an alternative and more accurate means of measuring cell movement, Spatio-Temporal Image Correlation
12 Spectroscopy (STICS) (Toplak et al., 2012; Meddens et al., 2016; Ashdown et al., 2017) was applied on a series of 2D
13 maximum intensity projections of 3D image stacks that were acquired via light-sheet microscopy (Zeiss Lightsheet Z.1;
14 Carl Zeiss, Jena, Germany) at different time points post-injury in *ex vivo* organ-cultured murine corneas. The raw data
15 consisted of a temporal sequence (i.e. time point per 2 hrs) of Z-stacks from corneas imaged through a 5×/0.16 detection
16 lens and 5×/0.1 illumination lens (pixel size 2.28 μm). The four fluorescent protein signatures were collected
17 sequentially as follows; CFP 445 nm excitation, 460-500 nm emission; GFP 488 nm excitation, 505-545 nm emission;
18 YFP 514 nm excitation, 525-545 nm emission; RFP 561 nm excitation, 575-654 nm emission. Z-stack images were
19 collected with an optimal sectioning step of 4.35 μm (proximally 550 slices). For every time point (Figure S1A), the
20 maximum intensity projection image was calculated along the Z-axis (Figure S1B). Although the data was acquired in
21 four channels, all intensities were combined to produce a single grayscale time series of maximum projection images in
22 the X-Y plane (Figure S1C). Image registration (Figure S1B; images superimposed) was performed using image cross-
23 correlation; this ensured alignment of every frame in the series to the first. STICS was then applied on the registered
24 maximum intensity projection time series, where the local region of interest was set to 64×64 pixels by 10 frames
25 (Figure S1C; data sub-voxel). Registered image series were Fourier filtered to exclude immobile components as
26 previously described (Toplak et al., 2012). For each voxel of data, STICS correlation function (CF) was calculated
27 (Figure S1C, 3 temporal lags CF; yellow colored rectangular prism). CF is the fit with a 2D Gaussian function at each
28 temporal lag, and the peak positions were further fitted to extract the flow vector (v_x , v_y) for each voxel (Figure S1D).
29 The spatial shift of 16 pixels in X and Y plane ensured over-sampling between adjacent regions which was used to filter
30 out erroneous flows. Briefly, the mean of 8 nearest neighbouring region speeds were compared to the central region
31 value and if outside the variance of the neighbourhood, the value was set to a not-a-number. To achieve the temporal
32 evolution of flow-map, 10 frames at a time were analyzed and the temporal block of images shifted by 1 frame (2 hrs)

1 to ensure continuous transition in flow per region of interest, and to also account for possible change in local flow
2 during the experiment. The resulting vector flow-map was obtained as result of spatio-temporal shift of data sub-voxel
3 (Figure S1E). Furthermore, to account for the 3D cellular movement on the surface of cornea, its curvature was
4 measured on the X-Z and Y-Z projections of the Z-stack (Figure S1F, red hatched lines). From the curvature traces, the
5 correction map was calculated (Figure S1G) which was used to correct the flow-map obtained from maximum
6 projections in X-Y plane (Figure S1E); this was subsequently converted into a vector flow-map of cells produced from
7 the movement on the curved surface defined by the cornea (Figure S1H). The corrected spatio-temporally resolved
8 vector flow-maps were further analyzed by combining the speed of cells at the leading edge of the wound, and their
9 histograms compared to those obtained for speed in the peripheral region. These analyses were conducted in custom
10 built software MATLAB (MathWorks, Natick, MA).

11

12 **Overview, design concepts and details of the mathematical model**

13 ***1. Purpose***

14 The model is used to investigate the role that population pressure-driven motility plays in corneal wounding and repair
15 and to compare spatial distributions of clonally related cells in corneas, following cases of no wounding and wounding
16 in a central circular format. It is based on a previous model (Grimm et al., 2010; Lobo et al., 2016).

17

18 ***2. Entities, state variables and scales***

19 The model space is a circular region representing the cornea and adjacent limbus, which collectively is in one of three
20 states: a ‘healthy state’, an ‘early wounded state’ and a ‘late wounded state’. The healthy state represents a cornea
21 whose dynamics do not incorporate any wound, or any active response to previous wounding. The early wounded state
22 represents a cornea that is undergoing repair, where the key driver of wound repair is cell movement into the vacant
23 wounded area, before the wound approaches closure. The late wounded state represents a cornea that has almost
24 transitioned into the healthy state, where the key component of wound repair is cells coming together spatially, which
25 results in wound closure.

26

27 Regardless of collective state of the cornea, the model consists of approximately 4,000 cells within the basal layer
28 inside a circular perimeter with a diameter of 115 idealized cell radii (defined below in ‘5. Initialization’). Each cell has
29 the following attributes or state variables:

- 30 1. Position: The position of a cell is determined by a single pair of co-ordinates, as we ignore the curvature of the
31 basal layer of the cornea. Collectively, the set of cell positions is used to determine the edges and vertices of cells,

- 1 using geometric structures known as Voronoi diagrams. We assume the limbus consists exclusively of stem cells,
 2 which are all within a single cell rim, a fixed distance away from the center of the corneal region.
- 3 2. Lineage identification: Each stem cell is endowed with a distinct lineage identification code, and all future
 4 progeny of that stem cell in the cornea share the same cell lineage identification code.
- 5 3. Age: Cells are attributed with a current age. Processes such as time to cell death, symmetric cell division and
 6 differentiation off the basal layer are assumed to occur approximately periodically.
- 7 4. Type: Each cell is characterized by a type that is used to reflect the phenotypic behavior of cells in the cornea, or
 8 to maintain the model. Cell types include: Ghost cells, whose position is exterior to the circular region that
 9 represents the cornea, and are designed to play no active part in corneal dynamics, but are necessary to maintain the
 10 spatial structure of the model; Blank cells, that represent wounded areas inside the circular region that are not
 11 occupied by other cell types; epithelial stem cells that represent the phenotypic properties of stem cells found in the
 12 limbus otherwise known as LESC; and TACs within the cornea. An injury transforms cells in the wounded area
 13 from TAC cells into Blank cells and moves the cornea from a healthy state to an early wounded state.
- 14 5. Cell types Blanks, LESC and TAC differ in the following way depending on the collective state:
- 15 5.1. Healthy state

	Blank ^a	LESC	TAC
Lifespan	n/a	Normally distributed $N(3000, 10)$	Normally distributed $N(300, 10)$
Replicative capacity	n/a	∞^b	TAC(max) = 3 ^c
Replicative Frequency	n/a	R^{*d}	$N(300, 10)^e$

- 16
- 17 a) Blank cells are not present in the healthy state
- 18 b) LESC; are assumed to have a replicative capacity that is much greater than the time scale represented by the
 19 model and are therefore characterized by limitless replicative potential for both symmetric and asymmetric
 20 proliferation in the model. LESC; are assumed to replicate symmetrically, producing two LESC; or
 21 asymmetrically, producing an LESC; and a TAC
- 22 c) TAC; can divide asymmetrically to produce another TAC and a TDC. TDC; do not contribute to the basal layer
 23 and are not depicted in simulations. TAC; have a limited number of rounds of symmetric cell division, known as
 24 TAC(max), after which they divide symmetrically to produce two TDC;.

d) The value of R^* , the replicative rate of LESC's are chosen to maintain equilibrium in cell population over time. This is determined by the model parameters and depends on the other parameters listed above.

e) At the end of their lifespan, TAC(n) cells divide symmetrically to produce two TAC($n-1$) cells when $n > 1$, or two TDC cells when $n = 1$.

5.2 Early and late wounded state

	Blank	LESC	TAC
Lifespan	Dependent on properties of the Blank cell ^a	Normally distributed $N(3000, 10)$	Normally distributed $N(300, 10)$
Replicative capacity	None	∞	TAC(max) = 3
Replicative Frequency	n/a	$2.5R^*$ ^b	$N(300, 10)$

a) In the early wounded state, cells in the circular region more effectively push into Blank cells than other cells in the cornea. This represents the preference for cells to move into unoccupied wounded areas of the cornea over competing for space with other cells. Blank cells remain in the cornea and may occupy less of the basal layer, but they are not yet removed. In the late wounded state, Blank cells are removed as follows:

b) Blank cells are further classified as internal Blank cells, which are only adjacent to other Blank cells, and edge Blank cells, which are adjacent to at least one TAC cell.

- When the distance between two internal Blank cells is small enough (less than 0.15 idealized cell radii), they are replaced by a single Blank cell whose position takes the value of the average position of the two internal cells being replaced

- The cornea moves from an early wounded state to a late wounded state when there are more edge Blank cells than internal Blank cells. When the cornea is in the late wounded state, Blank cells are removed stochastically with $p = 0.2$ per Blank cell per time step, and are not replaced.

c) LESC's have a 2.5-fold increase in proliferation as a response to wounding.

3. Processes overview and scheduling

At each step, the following processes occur in this order:

- 1 1. Cell motility
- 2 2. Possible wounding and changing the collective state to one of healthy, early wounding or late wounding
- 3 3. Remove Blank cells if in late wounding state
- 4 4. Render and record the state of the simulation
- 5 5. Cell division of LESC
- 6 6. Differentiation off the basal layer
- 7 7. Cell division of TACs

8

9 **4. Design Concepts**

- 10 1. Basic principles: We make the following assumptions
 - 11 a) The cornea is in a state of homeostasis, conforming with the X, Y, Z hypothesis (Thoft and Friend, 1983).
 - 12 b) The cell lineage pathways in the cornea are LESC-TAC-TDC
 - 13 c) There is a fixed population of LESC in the limbus
 - 14 d) The cells in the cornea are motile
 - 15 e) The population pressure is related to the density of neighboring cells
 - 16 f) Cells respond to pressure gradients by moving from higher pressure to lower pressure areas.
 - 17 g) TAC cells preferentially move to the direction of an adjacent Blank cell rather than other TACs or LESC.
- 18 2. Emergence: the spatial structures of cell lineages in the cornea emerge through passive motility rules, driven by a
19 cellular spring network.
- 20 3. Adaptation: cells in the cornea move in response to the pressure exerted by their immediate neighbors and either
21 replicate or die in response to reaching their lifespan; LESC respond to the death of a neighbor by replicating
22 themselves; these responses do not adapt over time or in response to position.
- 23 4. Objectives: the cells do not aim to meet any objectives.
- 24 5. Learning: individual cells do not change their adaptive traits over time in response to experience.
- 25 6. Prediction: there are no adaptive traits in the model, so the agents in the model do not make any predictions.
- 26 7. Sensing: cells can sense the pressure exerted by their neighbors and whether they are located in the limbus or the
27 cornea. Blank cells can sense whether their neighbors are TACs or other Blank cells.
- 28 8. Interaction: cells respond to the local configurations of other cells by moving in response to a pressure gradient
29 or, in the case of LESC, replicating in response to the death of a neighbor.

- 1 9. Stochasticity: the lifespans of cells are normally distributed for both LESC and TACs. The other source of
 2 stochasticity in the model occurs when a neighboring LESC is elected to undergo symmetric cell division in
 3 response to the removal (death) of a LESC.
- 4 10. Collectives: there is no pre-determined collective behavior in the model.
- 5 11. Observation: position, lineage identification code, age and proliferative capacity are recorded for all cells in the
 6 model at every time step.

7

8 **5. Initialization**

9 Cell positions are initially chosen so that the Voronoi diagram generated is a regular hexagonal grid (the distance
 10 between the positions of neighboring cells is a constant, s , known as the idealized cell diameter). All LESC are given a
 11 random age (uniformly distributed from 0 to their lifespan) and a unique cell lineage identification code. Initially, all
 12 TACs are not assigned a lineage identification code. TACs derived from LESC after initialization inherit the lineage
 13 identification code of their parent cell. Cell types are chosen such that LESC have only two adjacent LESC neighbors,
 14 and that TACs that have less proliferative capacity are placed towards the center of the cornea. The model is run for
 15 2000 pre-simulation time steps to achieve homeostasis. At this point, all cells have acquired a lineage identification
 16 code, and a stable spoke-like pattern has been achieved, and the simulation begins.

17

18 **6. Input**

19 There are no external input data that alter the model during the simulations.

20

21 **7. Sub-models**

22 Cell motility in response to pressure: the cell positions of all TACs are updated through a cell movement rule, which is
 23 applied 100 times per time step. Each time the movement rule is applied, the set of Voronoi neighbors (found through
 24 Delaunay Triangulation) is found, and cell movement arising from pressure between a TAC neighboring cell is
 25 proportional to the $d_p \cdot s_t$, where d_p represents the distance between the cell neighbors, and s_t varies depending on the
 26 types of cells that are neighbors as follows:

27

28

Cell type	Neighboring cell type	S_t
-----------	-----------------------	-------

LESCs or TACs	LESCs or TACs	s^a
TACs	Blank	$0.95 s^b$
Blank	TACs	$1.05s^b$
Blank	Blank	s_b^c

1

2 a) s is the idealized cell diameter

3 b) TACs preferentially move towards vacant areas of the cornea, and Blank cells in the wounded area move away from
4 this advancing frontier

5 c) s_b is determined dynamically to be the average Blank cell diameter that covers the current area of wound

6

7 The total movement of a cell is the sum of all movements arising from each pair of neighbors, and this is done
8 synchronously. The positions of both LESCs and Ghosts are fixed.

9 1. Cell motility: Cell positions are updated through the following movement rule which is applied 100 times per
10 time step

$$11 \quad \Delta p_i = \frac{1}{2\sqrt{3}} \sum_j w_{i,j} (p_i - p_j) (s_t - |p_i - p_j|) / |p_i - p_j|$$

12 2. Render and record the state of the simulation, collect all figures and data.

13 3. Age cells: All cells are assumed to age synchronously.

14 4. LESCs that have reached their lifespan are removed and are synchronously replaced by symmetric proliferation of
15 a neighboring LESC, which is chosen at random. The cell lineage identification of the new cell matches that of the
16 mother cell, and the lifespan of the new cell is chosen randomly from $N(3000, 10)$.

17 5. LESCs give rise to TAC(max)s at a rate designed to maintain corneal equilibrium. Newly proliferated TACs share
18 the lineage identification of the mother cell, its position is $0.5s$ closer to the center of the cornea than the mother cell,
19 and the lifespan of the TAC(max) is chosen randomly from $N(75, 25)$. While the cornea is wounded, this rate is
20 increased 2.5-fold.

21 6. When $s_b^c < 0.15s$, Blank cells are considered to be sufficiently small, are completely surrounded by other Blank
22 cells (known as internal Blank cells) and are deemed to be available for removal. Blank cells that are within $0.25s$ to
23 another Blank cell are removed leaving a singular, larger Blank cell. When there are no internal Blank cells, the
24 remaining Blank cells are removed stochastically with $p = 0.2$ per Blank cell per time step.

25 7. Cell differentiation off the basal layer: TACs that have reached their lifespan and exhausted their replicative

1 potential die by becoming TDCs in the suprabasal layers of the epithelium and are removed from the model.

2 8. Symmetric division of a TAC with x rounds of cell division remaining produces two daughter TACs, both having
3 $x-1$ potential rounds of cell division remaining. Both these daughter cells share the lineage identification code as the
4 mother cell and are placed within 0.5s of the position of the mother cell, with no other predetermined spatial
5 assignment.

6

7 **Supplementary References**

8 Abramoff, M.D., Magalhães, P.J., and Ram, S.J. (2004). Image processing with ImageJ. *Biophotonics international* 11,
9 36-42.

10 Ashdown, G.W., Burn, G.L., Williamson, D.J., Pandžić, E., Peters, R., Holden, M., Ewers, H., Shao, L., Wiseman, P.W.,
11 and Owen, D.M. (2017). Live-cell super-resolution reveals F-actin and plasma membrane dynamics at the T cell
12 synapse. *Biophysical journal* 112, 1703-1713.

13 Cruzat, A., Witkin, D., Baniasadi, N., Zheng, L., Ciolino, J.B., Jurkunas, U.V., Chodosh, J., Pavan-Langston, D., Dana,
14 R., and Hamrah, P. (2011). Inflammation and the nervous system: the connection in the cornea in patients with
15 infectious keratitis. *Investigative ophthalmology & visual science* 52, 5136-5143.

16 Di Girolamo, N., Bobba, S., Raviraj, V., Delic, N., Slapetova, I., Nicovich, P., Halliday, G., Wakefield, D., Whan, R.,
17 and Lyons, J. (2015). Tracing the fate of limbal epithelial progenitor cells in the murine cornea. *Stem cells* 33, 157-169.

18 Grimm, V., Berger, U., DeAngelis, D.L., Polhill, J.G., Giske, J., and Railsback, S.F. (2010). The ODD protocol: a
19 review and first update. *Ecological modelling* 221, 2760-2768.

20 Lobo, E.P., Delic, N.C., Richardson, A., Raviraj, V., Halliday, G.M., Di Girolamo, N., Myerscough, M.R., and Lyons,
21 J.G. (2016). Self-organized centripetal movement of corneal epithelium in the absence of external cues. *Nature*
22 *communications* 7.

23 Meddens, M.B., Pandzic, E., Slotman, J.A., Guillet, D., Joosten, B., Mennens, S., Paardekooper, L.M., Houtsmuller,
24 A.B., Van Den Dries, K., and Wiseman, P.W. (2016). Actomyosin-dependent dynamic spatial patterns of cytoskeletal
25 components drive mesoscale podosome organization. *Nature communications* 7.

26 Richardson, A., Lobo, E.P., Delic, N.C., Myerscough, M.R., Lyons, J.G., Wakefield, D., and Di Girolamo, N. (2017).
27 Keratin-14-Positive Precursor Cells Spawn a Population of Migratory Corneal Epithelia that Maintain Tissue Mass
28 throughout Life. *Stem Cell Reports* 9, 1081-1096.

29 Thoft, R.A., and Friend, J. (1983). The X, Y, Z hypothesis of corneal epithelial maintenance. *Investigative*
30 *ophthalmology & visual science* 24, 1442-1443.

- 1 Toplak, T., Pandzic, E., Chen, L., Vicente-Manzanares, M., Horwitz, A.R., and Wiseman, P.W. (2012). STICCS reveals
- 2 matrix-dependent adhesion slipping and gripping in migrating cells. *Biophysical journal* *103*, 1672-1682.